

1 **Selective Modulation Of A1 Astrocytes By Drug-**
2 **Loaded Nano-Structured Gel In Spinal Cord**
3 **Injury**

4

5

6 *Irma Vismara*^{1§}, *Simonetta Papa*^{1§}, *Valeria Veneruso*^{1,2}, *Emanuele Mauri*², *Alessandro*
7 *Mariani*³, *Massimiliano De Paola*³, *Roberta Affatato*⁴, *Arianna Rossetti*², *Mattia Sponchioni*
8 ², *Davide Moscatelli*², *Alessandro Sacchetti*², *Filippo Rossi*², *Gianluigi Forloni*¹, *Pietro*
9 *Veglianese*^{1*}

10

11 1 Department of Neuroscience, Istituto di Ricerche Farmacologiche Mario Negri IRCCS, via
12 Mario Negri 2, 20156 Milano, Italy;

13 2 Department of Chemistry, Materials and Chemical engineering “Giulio Natta”, Politecnico
14 di Milano, via Mancinelli 7, 20131 Milano, Italy;

15 3 Department of Environmental Health Sciences, Istituto di Ricerche Farmacologiche IRCCS
16 “Mario Negri”, via Mario Negri 2, 20156 Milan, Italy

17 4. Department of Oncology, Istituto di Ricerche Farmacologiche IRCCS “Mario Negri”, via
18 Mario Negri 2, 20156 Milan, Italy

19

20 *corresponding author: pietro.veglianese@marionegri.it

21 § contributed equally

22

23

24 **ABSTRACT**

25 Astrogliosis has a very dynamic response during the progression of spinal cord injury, with
26 beneficial or detrimental effects on recovery. It is therefore important to develop strategies to
27 target activated astrocytes and their harmful molecular mechanisms so as to promote a
28 protective environment to counteract the progression of the secondary injury. The challenge is
29 to formulate an effective therapy with maximum protective effects, but reduced side effects. In
30 this study a functionalized nanogel-based nanovector was selectively internalized in activated
31 mouse or human astrocytes. Rolipram, an anti-inflammatory drug, when administered by these
32 nanovectors limited the inflammatory response in A1 astrocytes, reducing iNOS and Lcn2,
33 which in turn reverses the toxic effect of proinflammatory astrocytes on motor neurons *in vitro*,
34 showing advantages over conventionally administered anti-inflammatory therapy. When tested
35 acutely in a spinal cord injury mouse model it improved motor performance, but only in the
36 early stage after injury, reducing the astrocytosis and preserving neuronal cells.

37

38

39 Spinal cord injury (SCI) is the most frequent disabling injury of the spine. SCI leads to cell
40 degeneration at the epicenter of the lesion, including neurons, astrocytes and oligodendrocytes.
41 ¹ Secondary processes (*e.g.* inflammatory response, excitotoxicity, apoptosis and oxidative
42 stress) cause additional loss of neurons and glial cells (secondary injury). The reactive
43 proinflammatory response of the astrocyte population, with the subsequent formation of scar
44 tissue and the inhibition of axonal regrowth, seems to be pivotal. After acute damage, astrocytes
45 become reactive and undergo a spectrum of changes in their phenotype, gene expression and
46 proliferation. ² It has been suggested that reactive astrocytes near the lesion might have roles
47 that are either beneficial or detrimental in **central nervous system (CNS)** repair. ^{1,2} Several
48 neuropathological stimuli induce a variable phenotypic “state” of astrocytes that change after
49 injury. These are commonly called stated A1 and A2 ^{2,3} and are parallel to the terminology of
50 macrophages M1 and M2, which was applied to the microglial response in the CNS. ⁴
51 Astrocytes with A1 phenotype exert neurotoxic effects, upregulating many genes associated
52 with the synapse and neuronal degeneration, suggesting that A1 has harmful “**pro-**
53 **inflammatory**” action. ^{2,3} In contrast, A2-induced reactive astrocytes exert protective effects by
54 upregulating the expression of neurotrophic factors that promote neuronal survival and
55 regrowth. ^{2,3}
56 Various approaches have been employed to counteract the negative effects of activated
57 astrocytes ⁵, blocking scar formation or pharmacologically and genetically reducing
58 upregulation of axon growth inhibitors. ^{6-8,9} However, genetic manipulation is not clinically
59 feasible, because ethical issues remain and it could have side effects, whereas pharmacological
60 treatment could act on unwanted common mechanisms without any selective effect on
61 astrocytes. Innovative biomaterial technologies have been developed to induce spinal cord
62 regeneration and improve functional outcomes after injury ¹⁰⁻¹⁴. Polymeric **nanoparticles (NPs)**
63 with their versatility in size, potential surface and hydrophilic or lipophilic characteristics, offer

64 considerable advantages in drug delivery, increasing the selectivity of drugs and controlling
65 their release overtime. In the past decade a large number of different NP systems have been
66 tested in SCI, but only a few are directed to astrocytes, and none are selective for them.^{6,15,16}
67 We have focused on a specific category of NPs that, with their ability to swell, are commonly
68 referred to as nanogel (NG).¹⁷ Their advantages, compared with NPs, lie in greater colloidal
69 stability due to higher affinity for water, together with longer retention of their cargo, and easy,
70 reproducible synthesis.¹⁷
71 We have now developed and characterized a novel pharmacological delivery tool based on an
72 NG (polyethylene glycol (PEG) and polyethylene-imine (PEI)) coated with primary amines and
73 loaded with a drug (Rolipram) to obtain selective, controlled release for the astrocytic
74 component of the spinal cord.

75

76 RESULTS

77

78 *1. NG synthesis and characterization*

79 NG was synthesized by the CH₂Cl₂-in-water emulsification-evaporation method:
80 “Carbonyldiimidazole (CDI) activated” PEG was dissolved in the organic phase, and PEI was
81 dipped in aqueous solution. After sonication, the progressive evaporation of CH₂Cl₂ in the
82 emulsion status take place. The system can ensure homogeneous dispersion of PEG chains
83 around PEI promoting the interactions among the imidazole and amine moieties of the two
84 polymers, giving rise to the formation of carbamate bonds and entanglement of the chains. Then
85 grafting the terminal amine moieties in already formed NG was done in a single step through
86 the direct addition of 3-bromopropylamine to the NG solution. A reaction scheme for the NG
87 is reported in Figure S1. The 3-bromopropylamine nucleophilic substitution occurred on the
88 residual PEI amine groups and this reaction did not affect the NG bonds, preserving the

89 structural organization of the polymeric chains. The evidence of the system stability after
90 coating relies on the fact that NGs are still present as visible from AFM (Atomic Force
91 Microscopy) (Fig.S2). Carbamate bonds are indeed the crosslinking connections among PEG
92 and PEI chains so, in case of their break, the NG structure would have been no more consistent
93 and the polymers would have been dispersed in the water medium.

94 No competition was observed between this reaction and the NG structural bonds, as
95 demonstrated by the preservation of the corresponding signals in NMR and FT-IR analyses
96 (Fig.S3, S4), after coating. The NG physical features were investigated using dynamic light
97 scattering (DLS) technique: the recorded data of NGs dissolved in PBS on size (diameter) and
98 z-potential are respectively 155 nm (PDI = 0.15) and 3.1 mV. The distributed positive charge
99 was related to the presence of -NH₂ surface groups that gave rise to NG protonation and a
100 positive charged interface.

101

102 ***2. Cellular uptake study of NG in murine astrocytes in vitro***

103 We examined the uptake of biodegradable NG (covalently linked to Cy5) in primary co-cultures
104 of microglia, astrocytes and neurons from the spinal cords of mouse embryos. A specific
105 antibody was used to detect neurons (SMI32) in co-culture with astrocytes; astrocytes and
106 microglia were analyzed in monoculture. “Pro-inflammatory” phenotype was induced by
107 treatment with lipopolysaccharide (LPS) for mono and co-cultures. After 24h exposure to NP,
108 a large amount of NG-based NPs was internalized into the cytosol on the outer nucleus in
109 astrocytes (Fig. 1; A, a). In contrast, when we analyzed activated microglia there were only a
110 few internalized NG (Fig.1; A, b), and none in neurons (Fig.1; A, c). We quantified the
111 internalized NG as a ratio between the NG signal area and cell area, confirming that a larger
112 amount of NG was taken up by activated astrocytes (Fig.1; A, d).

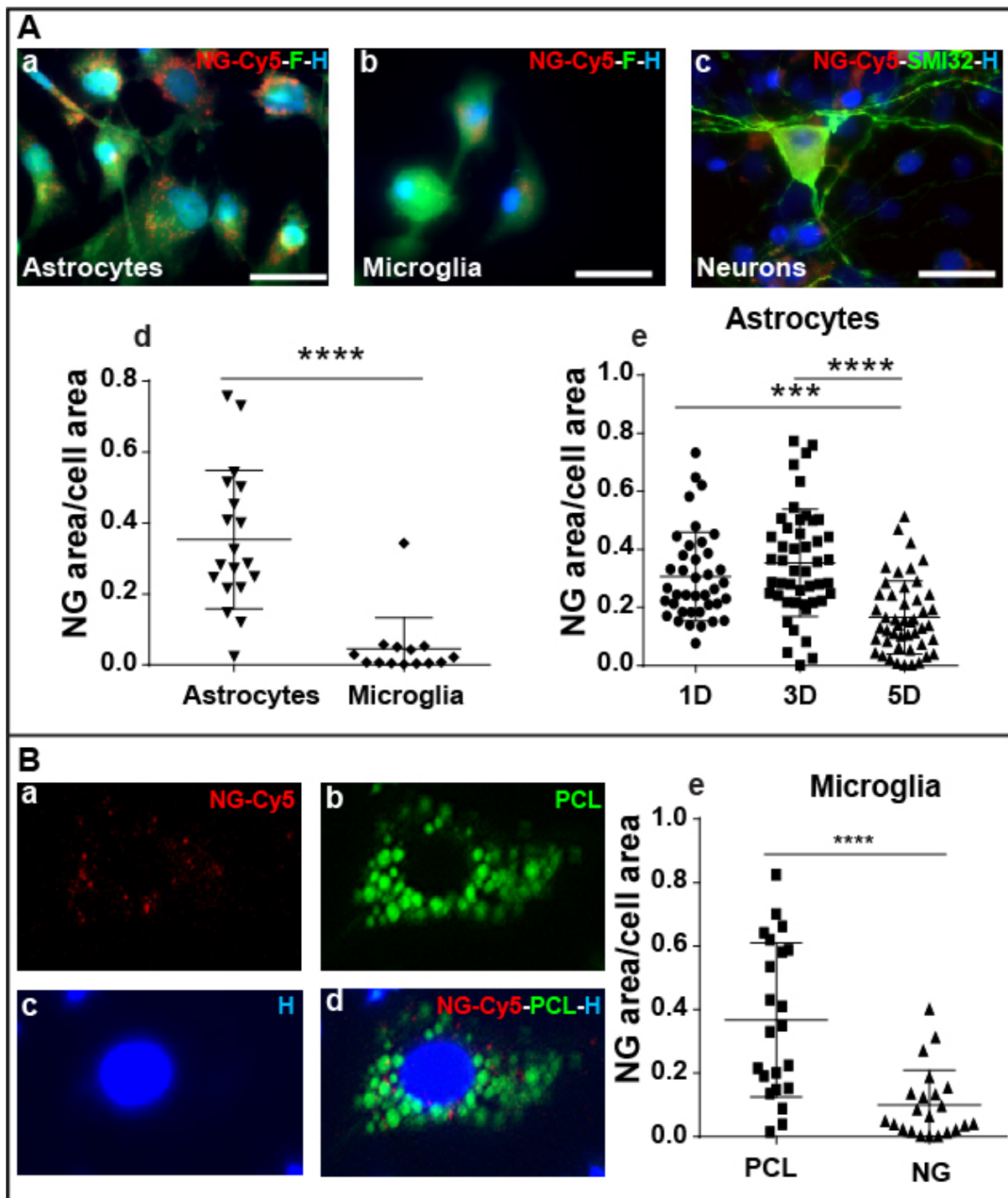
113 To confirm the reduced ability to internalize NG, we compared the amount of poly-methyl
114 methacrylate-(PCL), a nanovector selectively internalized in activated microglia¹⁸, and found
115 a significantly lower uptake for NG compared to PCL in the same cells (Fig.1; B, a-e). These
116 data suggest greater tropism of NG for activated astrocytes than microglia or neurons *in vitro*.
117 Time-lapse analysis was used to investigate the kinetics of internalization of NG in astrocytes.
118 NG uptake was already detectable after 24 hours of treatment, reaching the maximum signal,
119 which did not significantly change three days after the exposure. At five days the NG signal
120 decreased, demonstrating degradation of the nanovector (Fig.1; A, e).

121 In order to investigate targeting of the NG to activated phenotypes, we compared untreated
122 (CTR) (Fig. S5; A, a, B, a), LPS-treated (Fig. S5; A,B, b) and FGF (A2 stimuli) (Fig. S5; A, c)
123 or IL-4 (M2 stimuli) (Fig. S5; B, c) treated murine astrocytes or microglia *in vitro*.
124 Quantification of the NG uptake in murine astrocytes and microglia shows higher NG
125 internalization in LPS treated cells compared to CTR and FGF/IL-4 (Fig. S5; A, d, B, d). This
126 suggests a stronger treatment for the proinflammatory phenotype enhancing the selective
127 action.

128

129

130



131

132

133

134 **Figure 1**

135 *A) Characterization of NG uptake in primary cultures of (a) astrocytes, (b) microglia (c)*
 136 *neurons. A large amount of NG is located in the cytosol of astrocytes after 1 day (1D) of*

137 exposure. a) astrocytes or b) microglia stained by fluorescein (F, green); c) neurons stained
138 by SMI32 (SMI32, green); NG conjugated with Cy5 (NG-Cy5, red); cell nuclei stained by
139 Hoechst (H, blue). Scale bar 25 μ m. (d) Quantification of the NG uptake in activated
140 astrocytes and microglia shows higher NG internalization in astrocytes. (e) Quantification of
141 NG uptake in astrocytes 1, 3 or 5 days after exposure. At 5 days the NG signal is reduced by
142 degradation of the nanovector.

143 B) Quantification of NG uptake (a, d, red) vs PCL (b, d, green) in activated microglia. (e)
144 significantly lower uptake was for NG than PCL in activated microglia.

145 Data are mean \pm SD. Mann-Whitney test (A, d, B, e) and one-way ANOVA followed by
146 Bonferroni's post hoc test (A, e). Statistical significance: (***) $p \leq 0.001$; (****) $p \leq 0.0001$.

147

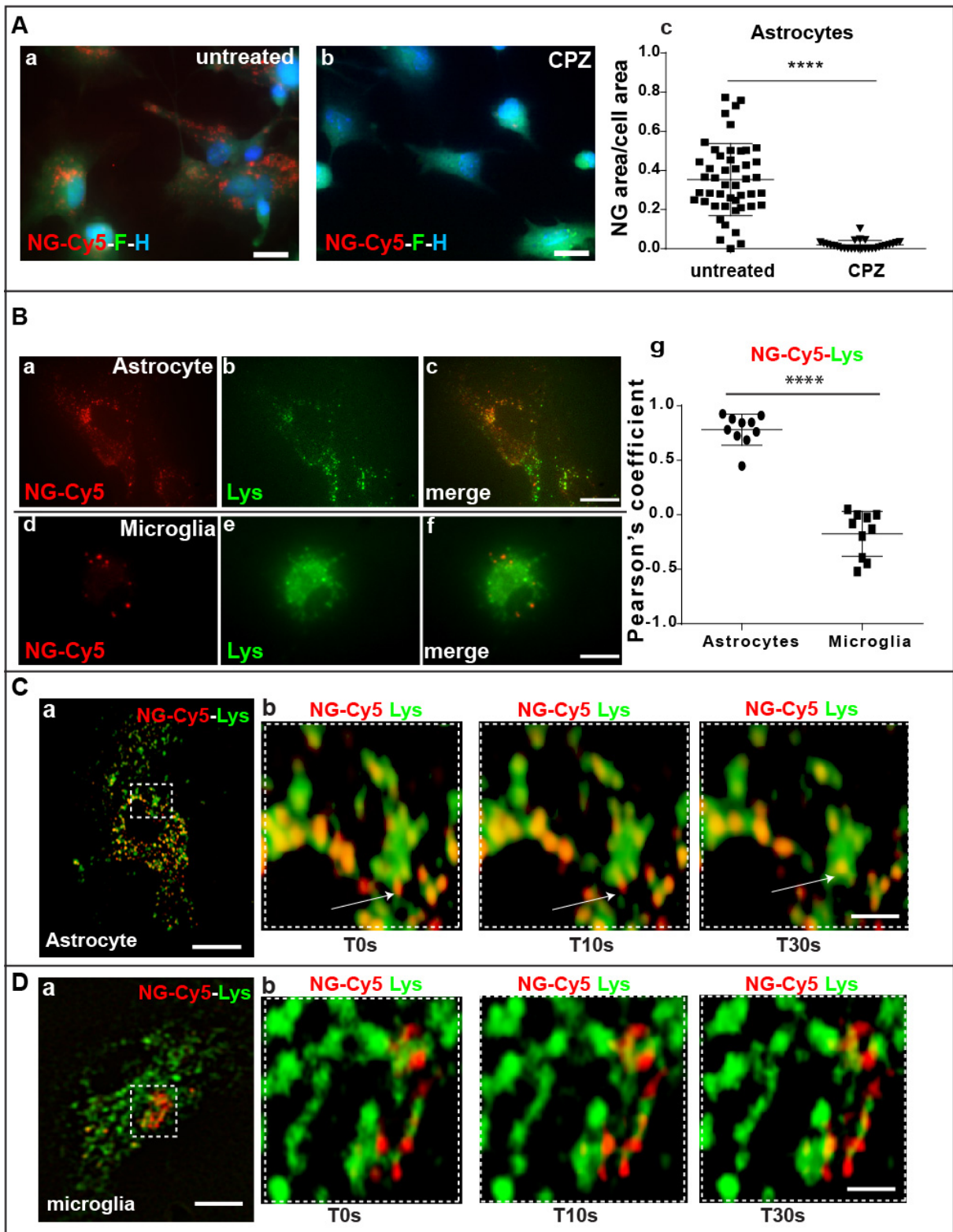
148 3. NG internalization and degradation in mouse astrocytes in vitro

149 To investigate the mechanisms of NG uptake into the astrocytes, we studied NG internalization
150 after 2h pretreatment with chlorpromazine (CPZ, a clathrin-mediated endocytosis inhibitor).

151 Quantification of the NPs in the cytosol showed a significant reduction of the Cy5 signal in
152 CPZ treated astrocytes compared to cells not treated with CPZ (Fig.2; A) suggesting that a
153 mechanism of clathrin-mediated endocytosis was involved in NG uptake. Clathrin-mediated
154 endocytosis can lead to degradation by lysosomes. To study the involvement of lysosomes in
155 the degradation after NG internalization we used a fluorescent indicator (lysosensor, Lys) to
156 test the activity of the lysosomal acidification machinery. Three days after NG exposure we
157 detected evident lysosomal enzymatic activity (fluorescent green signal), closely colocalized
158 with NG (fluorescent red signal) (Fig.2; B, a-c; C, a, b) confirming degradation by lysosomes
159 in astrocytes.

160 To verify whether the small number of NG in the microglial cells were degraded through
161 lysosomal activity, we studied the colocalization of the NG and Lys signals in microglia. NPs

162 did not show any sign of colocalization with Lys in microglia and in fact the NG signal was
163 dispersed in the cytosol (Fig.2; B, d-f; D, a,b); this was also demonstrated by quantitative
164 analysis where no colocalization was detected with Pearson's coefficient (Fig.2; B, g). This
165 suggests that the amount and mechanism of internalization/degradation in the microglia were
166 different from astrocytes, without any involvement of the clathrin-mediated endocytosis and
167 lysosomal degradation machinery that is instead normally involved in the NP
168 internalization/degradation of microglia.
169



170

171

172

173

174 **Figure 2**

175 A) Pretreatment with chlorpromazine (CPZ) inhibits NG uptake (red) into LPS-activated
176 astrocytes (b) compared to untreated LPS-activated cells (a) stained with fluorescein (F, green)

177 Scale bar A 5 μ m.

178 B) A colocalized signal between NG and the lysosensor indicates that NG is degraded by
179 lysosomal activity in astrocytes (a, b, c). NG (red) showed no colocalization with lysosomes
180 (green) in microglia (d, e, f). This was confirmed by quantitative analysis, using Pearson's
181 coefficient (g) Scale bar B 15 μ m.

182 C) Time-lapse analysis demonstrates colocalization of NG (a, b red) with lysosomes (a, b,
183 green) only in astrocytes (arrow indicates entrapment of NG into a lysosome vesicle during the
184 interval) D) but not in microglia (s=seconds) Scale bar C ,D 3 μ m.

185 Data are mean \pm SEM. **Mann-Whitney test**. Statistical significance: (****) $p \leq 0.0001$.

186

187 **4. Cellular uptake and degradation study of NG in “iPS-derived” human astrocytes in vitro**

188 To demonstrate that our nanovector-based delivery strategy is applicable in human cells, we
189 treated “iPS derived” human astrocytes with NG. Human astrocytes were prestimulated with
190 LPS for 18 hours then exposed to NP for 24 hours. A large amount of NG-based NPs was
191 internalized in the cytosol, with a distribution comparable to murine astrocytes (Fig. 3 a). Time-
192 lapse analysis was used to record the internalization of NG in human astrocytes. NG was
193 already taken up after 24 hours, reaching the maximum signal, which completely disappeared
194 three days after the exposure (Fig.3 b).

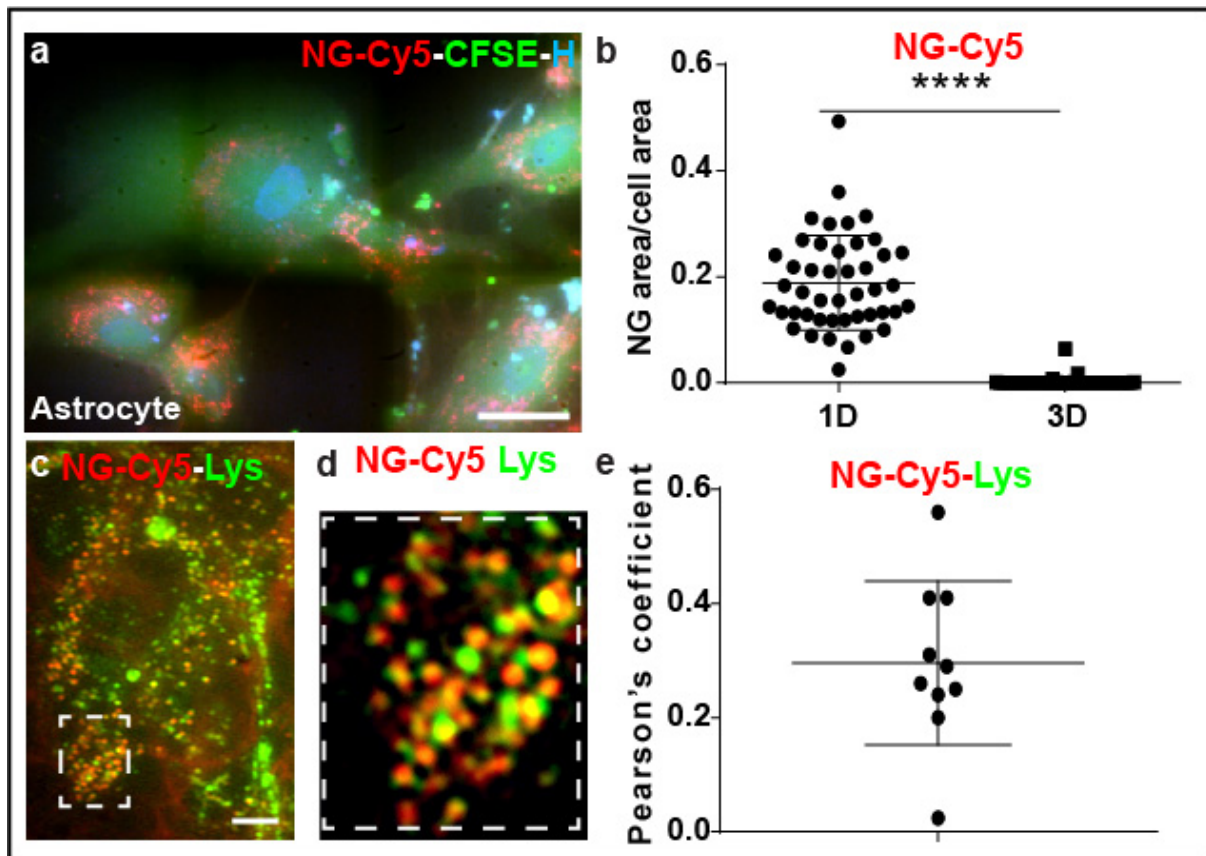
195 In order to investigate targeting of the NG to activated phenotype, we compared untreated
196 (CTR) (Fig. S5; C, a), LPS-treated (Fig. S5; C, b) or FGF (A2 stimuli) (Fig. S5; C, c) treated
197 human astrocytes in vitro. Quantification of the NG uptake shows higher NG internalization in
198 LPS treated cells compared to CTR and FGF groups (Fig. S5; C, d). This in line with the

199 treatment of murine astrocytes, where the pro-inflammatory phenotype will receive a stronger
200 treatment.

201 To demonstrate that the NG degradation was lysosomal as in murine astrocytes, we used the
202 lysosensor to test the activity of the lysosomal acidification machinery. One day after the NG
203 treatment we found remarked lysosomal activity (green fluorescent signal) colocalized with
204 NG (red fluorescent signal) (Fig.3 c,d) and quantified by Pearson's coefficient (Fig.3 e),
205 confirming that degradation by lysosomes occurred in human astrocytes.

206

207



208

209

210 **Figure 3**

211 a) NG uptake in iPS human-derived astrocytes. There was a large amount of NG in the cytosol
 212 of cells one day (1D) after the exposure. Astrocytes stained by CFSE (green); NG conjugated
 213 with CY5 (NG-CY5, red); cell nuclei stained with Hoechst (H, blue). Scale bar 5 μ m.

214 b) Quantification of NG uptake into LPS-activated human astrocytes indicates high NG
 215 internalization after one day (1D) of exposure. By three days (3D) NG are completely
 216 degraded. Scale bar 2 μ m.

217 c,d) Time lapse analysis shows colocalization of the NG signal with the lysosensor (Lys, green),
 218 confirming that the nanovector degradation involves lysosomes. Colocalization is quantified
 219 by Pearson's coefficient. Each of the points refers to Lys/NG-RhB signal ratio of individual

220 cells (e). Data are mean \pm SEM. Student's T-test. Statistical significance: (****) $p \leq 0.0001$.

221 Scale bar 1 μ m

222

223 5. In vitro drug delivery by NG in murine astrocytes

224 To investigate the ability of NG to deliver molecules into the astrocyte cytosol, NG were loaded

225 with a "drug mimetic" compound (To-pro3, a cell membrane impermeable fluorophore with

226 far-red emission). After 24 hours from exposure to To-pro3-loaded-NG, a clustered signal was

227 seen in the astrocyte cytosol. The colocalization of fluorescent Rhodamine B-positive NG (NG-

228 RhB red signal) with To-pro3 (green signal) showed that the mimetic drug was efficiently

229 encapsulated (Fig.4 a,b,d). In addition to the colocalized signal, a diffused To-pro3 staining

230 was found in the cytosol suggesting that a delivery of this compound occurred (Fig.4 a-d).

231 To confirm the delivery of To-pro3, we reconstructed the isosurface of the red (RhB-positive

232 NG) and green (To-pro3) signals and quantified their colocalization by Pearson's coefficient:

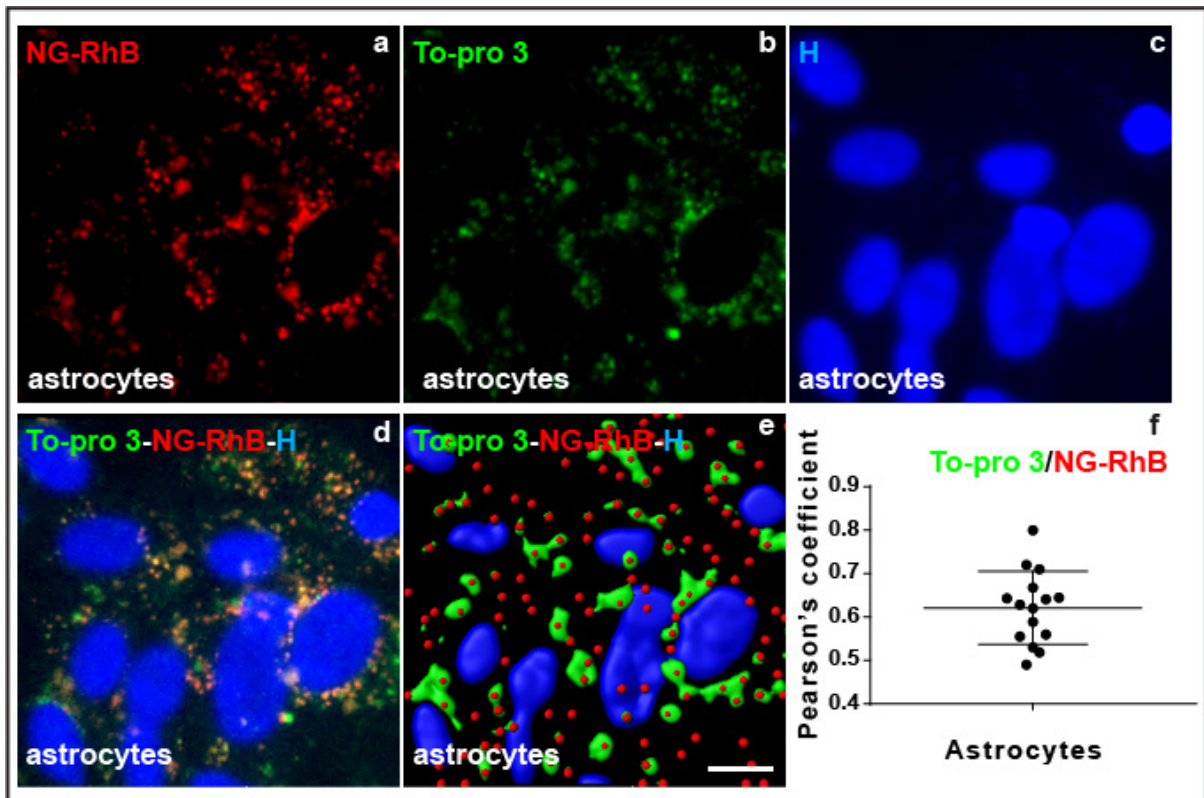
233 part of the To-pro3 signal diffused into the cytosol, overlapping RhB-positive NG (Fig.4 e-f).

234 To exclude any free crossing of To-pro3 in cells permeabilized due to damage of the membrane,

235 we evaluated only viable cells that were also impermeable to propidium iodide, used to test the

236 integrity of the extracellular membrane.

237



238

239 **Figure 4**

240 *To-pro3* (b, d, e, green) delivery from NG (a, d, e, red) after internalization in astrocytes.
 241 Astrocytes give a colocalized signal for *To-pro3* and RhB positive NG in the cytosol (a–d).
 242 Hoechst was used to stain the astrocyte nucleus (H, blue). A marked diffused signal of *To-pro3*,
 243 not colocalized with NG, is evident in the cytosol of astrocytes five days after NP exposure (d).
 244 (e) Isosurfaces reconstruction of the red (RhB-positive NG)/green (*To-pro3*) signal and (f)
 245 quantification of their partial colocalization. Individual data points are referred to *To-*
 246 *pro3/NG-RhB* signal ratio of individual cells. Scale bar 5 μ m.

247

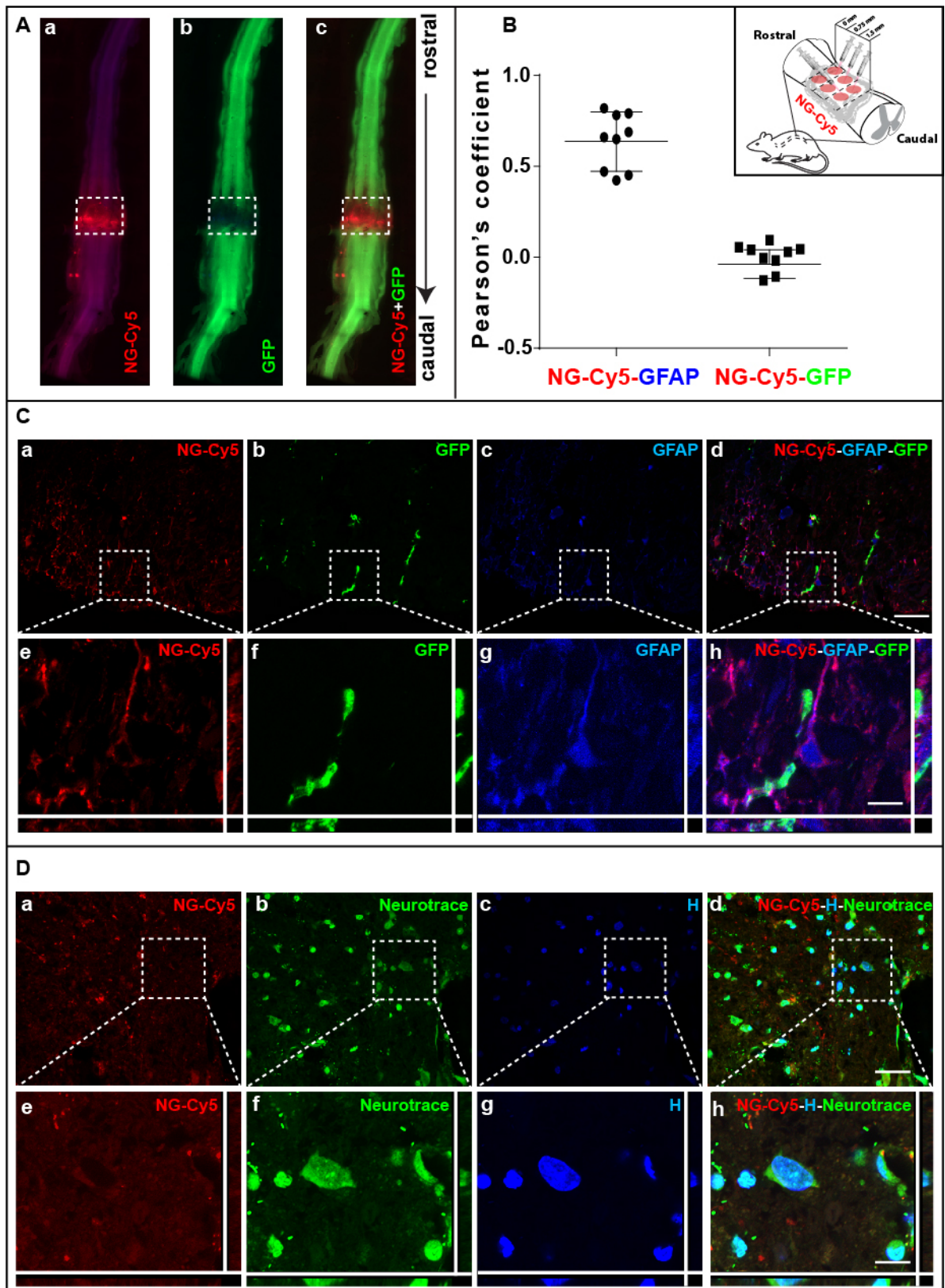
248

249 **6. Cellular uptake of NG *in vivo***

250 To validate and characterize the distribution of NG *in vivo*, we injected the nanovector into the
251 parenchyma of the damaged spinal cord 24h after the trauma (Fig.5 A). The six injections into
252 the spinal cord distributed over a longitudinal distance of $1320 \pm 266 \mu\text{m}$ (Fig.5 B, a-c). Three
253 days after the injection, we analyzed the tissue to examine the internalization of the NG, with
254 double staining, with markers for astrocytes (GFAP) or microglia (CX3CR1-GFP mice) or
255 neuronal cells (neurotrace), to demonstrate the cellular distribution of the nanovector. Some
256 hypertrophic astrocytes and activated microglial cells were detected in the damaged spinal cord,
257 with an early inflammatory response in the injured site (Fig.5 C, b,c,d,f,g,h). In the epicenter
258 of the lesion NG was mostly internalized into astrocytes, as evident from the colocalization
259 signal of GFAP and Cy5 conjugated with NG (Fig.5 C, a-h); no signal was detected in neurons
260 (Fig.5 D, a-h). Only a few microglia were positive for some NG in the more damaged part of
261 the spinal cord, suggesting that these cells might have more permeabilized membranes (data
262 not shown). These data validated *in vivo* the previous *in vitro* experiments, demonstrating again
263 the diffuse uptake in activated astrocytes in this SCI animal model, whereas internalization was
264 limited in a few microglia, but not in neurons.

265

266



267

268

269

270

271 **Figure 5**

272 A) Microscopy of the whole spinal cord 2h after the injection of NG and relative signal
273 amplitude (microglia, **CX3CR1 GFP-positive** in green; NG-Cy5, red). **B) Colocalization**
274 **analysis quantified by Pearson's coefficient (nine sampled sections in the site of injection were**
275 **analyzed). NG-Cy5 markedly colocalized with GFAP, whereas NG-Cy5 vs GFP was much less**
276 **or no detected. Insert shows NG injections with a distance of 0.75 mm from each other in the**
277 **lumbar tract of the spinal cord (T12-L1).** C,D) High magnification of spinal cord sections
278 show NG internalized into astrocytes (C; a,c,d,e,g,h), but not into microglia (C; a,b,d,e,f,h) or
279 neurons (D; a,b,d,e,f,h). Scale bar C, D 10 μ m.

280

281

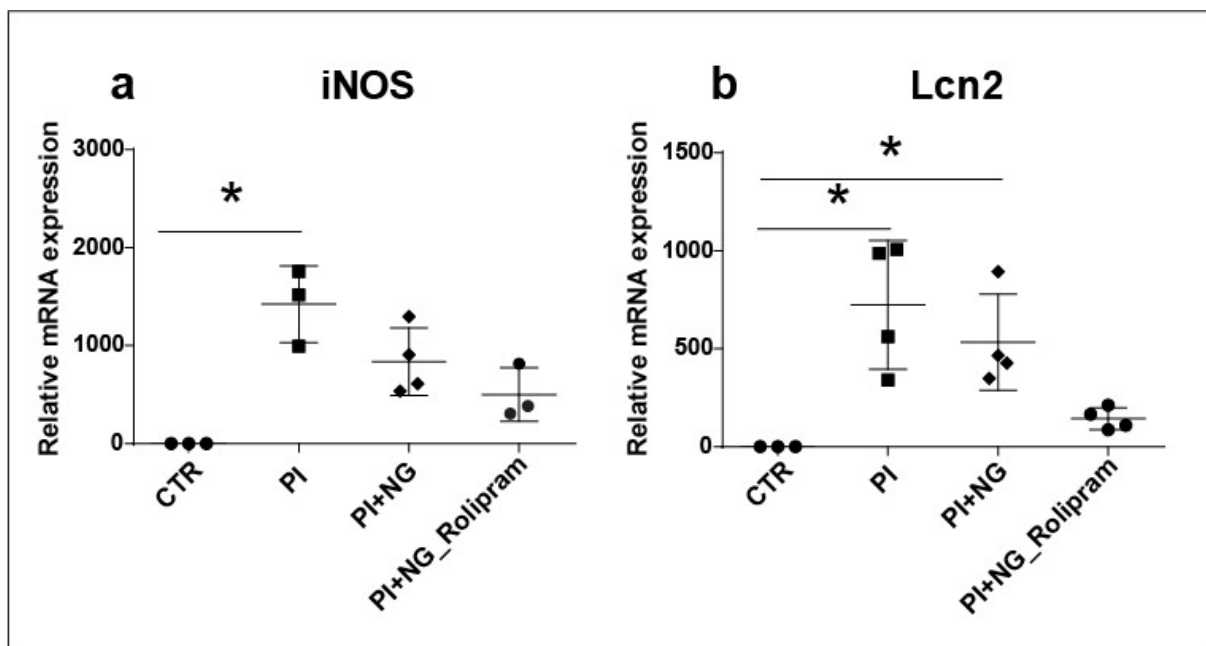
282 **7. Pharmacological activity of Rolipram delivered by NG in **murine** A1 astrocytes in vitro**

283 To demonstrate the ability of NG to deliver functional drugs, we studied Rolipram, an anti-
284 inflammatory drug, acting on the NF-kB pathway in astrocytes *in vitro*. **First we characterized**
285 **the drug release kinetic in vitro. Rolipram is released from NG with a characterized biphasic**
286 **pattern (Fig. S6). An initial burst release followed by a slower sustained release phase was seen**
287 **in 14 days (Fig. S6). The percentage of Rolipram released in the first 2 hours (around 30%) can**
288 **be attributed to the unloaded Rolipram and to the high initial concentration gradient present**
289 **(Fig. S6).**

290 In order to demonstrate the pharmacological activity, we treated astrocytes with three factors
291 (C1q 400 ng/mL, TNF α 30 ng/mL and IL1 α 3ng/mL; hereafter termed pro-inflammatory, PI),
292 that stimulate a specific pro-inflammatory response in astrocytes (A1 status).² Rolipram was
293 tested at 0.14 mg/mL, 0.033 mg/mL, 0.023 mg/mL and 0.014 mg/mL (**Fig.S7**). Real time
294 analysis of the homogenate of astrocytes exposed for 24h with PI showed that inducible nitric
295 oxide synthase (iNOS), a proinflammatory cellular signaling molecule, and Lipocalin 2 (Lcn2),

296 an inducible factor that is secreted by reactive astrocytes, that is toxic to neurons, were
297 significantly higher than in untreated culture (CTR) (Fig.S7). Significant differences were
298 found in the expression of iNOS compared to the CTR when we cotreated astrocytes with
299 PI+Rolipram at the lowest concentration (0.014 mg/mL), whereas co-treatment with Rolipram
300 at higher concentrations (starting from 0.023 mg/mL) was able to counteract the PI status.
301 Significant differences were found for Lcn2 for the highest concentration of Rolipram (0.14
302 mg/mL) compared to CTR. To demonstrate the ability of NG to load Rolipram and exploit its
303 anti-inflammatory effect, we used the concentration of the drug that had no significant effect
304 on both iNOS and Lcn2. We evaluated 0.014 mg/mL Rolipram loaded into NG, and found that
305 drug internalized by NG reduced iNOS and Lcn2 transcript *in vitro* in PI treated astrocytes
306 compared to PI alone (Fig.6). However, when we tested the single treatment with NG, iNOS
307 was also reduced, but not comparably to Rolipram-loaded NG treatment. This suggests that NG
308 can effectively deliver compounds into activated astrocytes and maximize their
309 pharmacological effects.

310



311

312

313 **Figure 6**

314

315 *Quantitative mRNA analysis of iNOS (a) and Lcn2 (b) expressed by astrocyte cultures after*
316 *treatment with PI (C1q, IL1 α and TNF α), used as positive control, or PI and NG or PI and*
317 *Rolipram loaded in NG. Data are mean \pm SD. Mann-Whitney test. Statistical significance: (*)*
318 *$p < 0.05$.*

319

320

321 **8. Rolipram-loaded NG reverses the toxic effect of proinflammatory murine astrocytes on**
322 **motor neurons in vitro**

323 We examined whether conditioned medium (CM) from pro-inflammatory astrocytes pretreated
324 with NG or Rolipram-loaded NG improved the damage response on cultured motor neurons. A
325 proinflammatory astrocyte phenotype (A1) was induced by 24h treatment with PI stimuli
326 defined above.² Stereology for unbiased cell counting of motor neurons was done after
327 neurofilament immunostaining (SMI32).¹⁹ First, we demonstrated the susceptibility of motor
328 neurons to CM from astrocytes treated for 24h with PI; they showed more - but not significant
329 -, neuronal death after 24h than with control medium (untreated astrocytes, CTR) (Fig.S8 a,b,e).
330 Rolipram-loaded NG (NG 0.0005 mg/mL, Rolipram 0.014 mg/mL) significantly preserved
331 motor neuron viability compared to PI (Fig.S8; b,d,e), whereas NG treatment did not give any
332 significant difference from the PI treated motor neurons (Fig.S8; b,c,e).

333 To see whether a few internalized NG or NG-Roli found in microglia acted on the pro-
334 inflammatory status of the microglia, we compared CM harvested from untreated microglia
335 (CTR), microglia treated with LPS, microglia co-treated with LPS and NG (LPS-NG) or
336 microglia co-treated with LPS and Rolipram-loaded NG (LPS-NG_Roli) on cultured motor
337 neurons (Fig.S9). We found no differences among the treatments, with comparable amounts of
338 motor neurons. Overall these data suggest that only Rolipram-loaded NG pre-treated astrocytes
339 improve neuronal survival reducing the deleterious inflammatory paracrine effect.

340

341

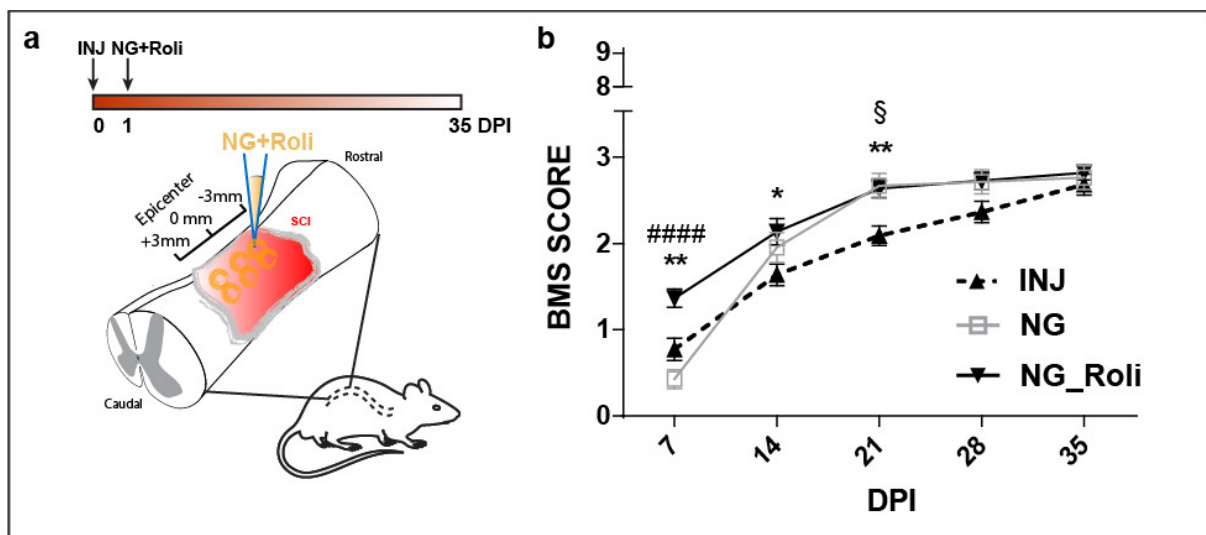
342 **9. Rolipram-loaded NG improves functional recovery only early after SCI in vivo**

343 To test the effect of Rolipram delivered by NG in SCI, we ran *in vivo* experiments. Mice were
344 randomly distributed into three groups and subjected to SCI: untreated (INJ), treated with NG
345 or Rolipram-loaded NG (NG-Roli) one day post-injury. Six injections with a glass capillary

346 were made into the damaged spinal cord to administer NG (0.025 mg/mL) or NG-Roli (Nanogel
347 0.025 mg/mL, Rolipram 0.7 mg/mL) (Fig.7 a). We rated behavior with the Basso mouse scale
348 (BMS) weekly up to 35 DPI (Fig.7 b).

349 In the NG-Roli treated group, there was significant motor functional improvement from 7 to 21
350 DPI compared to the INJ group (Fig.7 b). After 28 DPI up to 35 DPI motor performance was
351 no longer different from the untreated injured group (Fig.7 b). We also noted a significant
352 behavioral improvement for the NG-Roli treated group compared to the NG group at 7 DPI,
353 that became no longer different from 14 to 35 DPI (Fig.7 b). The NG treated group showed
354 some motor recovery at 21 DPI compared to the untreated injured mice (Fig.7 b). These results
355 suggest that Rolipram had an effect only at 7 DPI after the treatment, in an initial acute-subacute
356 phase, compared to NG treated mice, and from 7 to 21 DPI compared to untreated mice. NG
357 also served to regain partially motor control at 21 DPI, suggesting an effect on astrocytes.

358



359

360 **Figure 7**

361 *Early treatment with NG loaded with Rolipram improved locomotor performance in SCI mice:*

362 *a) injection of NG loaded with Rolipram in SCI mice at 1 DPI. b) SCI mice untreated (INJ) or*

363 *treated with NG (NG) or NG loaded with Rolipram (NG_Roli), examined weekly starting 7*

364 days post-treatment, rated on the Basso Mouse Scale - BMS (score 0, complete paralysis, score
365 9, complete mobility, compared to healthy mice). Locomotor performance significantly
366 improved in NG_Roli mice compared to the INJ group from 7 to 21 DPI (*) and compared to
367 NG at 7 DPI (#). NG treatment gave significant improvement in locomotor performance at
368 21 DPI compared to the INJ group (§).

369 Data are mean \pm SEM. One-way ANOVA followed by Bonferroni's post hoc test was applied.

370 Statistical significance: (* and §) $p < 0.05$, (**) $p < 0.01$, (####) $p < 0.0001$; $N = 12$ mice/ group.

371

372 **10. Rolipram-loaded NG preserved neurons and reduced astrocytosis in vivo**

373 Recovery after treatment with Rolipram-loaded NG was assessed by evaluating neuronal
374 preservation and the level of astrocytosis in the injured spinal cord. We used quantitative
375 stereological analysis to record the number of neurons (NeuN positive cells) (Fig.8 A) and
376 astrocytes (GFAP positive cells) (Fig.8 B) in the tissue. We examined an untreated injured
377 group (INJ) or Rolipram-loaded NG (NG_Roli) treated mice at 14 DPI. An area around the
378 epicenter of the lesion (-1.3/+1.5 mm rostro-caudal) was examined (Fig.8 A, a, B, a). Loss of
379 nervous tissue, impairing recovery ability and functional activity was recorded in the epicenter
380 of the lesion in the INJ group (Fig.8 A, b,d,e). With the NG_Roli treatment, neurons were more
381 preserved, and quantitative analysis indicated a significantly larger number of neurons
382 compared to INJ mice (Fig.8 A,b,c,d,e). Neuronal survival in relation to their distance from the
383 injured epicenter have been showed (Fig.8 A, d). This suggests that more neuronal cells are
384 preserved in the caudal tract than rostral part of the spinal cord.

385

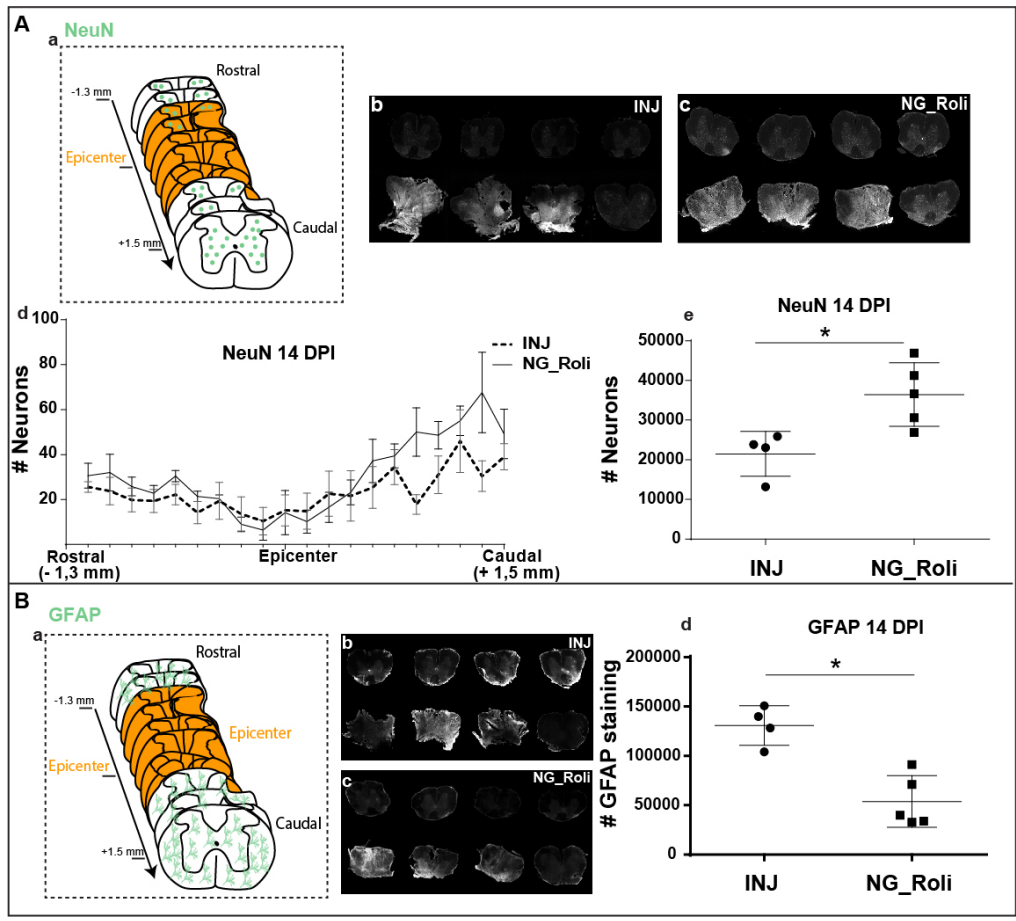
386 Neuronal survival was also investigated at 63 DPI. We analyzed the motor behavior up to
387 63 DPI. In this paper we showed up to 35 DPI because from 35 to 63 DPI no difference was
388 found. On the contrary to 14 days post injury, we did not find a significant difference of

389 neurons by comparing untreated injured mice (INJ) with Rolipram-loaded NG treated mice
390 (NG_Roli) (Fig. S10). This in line with the results in vivo confirming a lack of a long lasting
391 effect of the Rolipram-loaded NG treatment.

392 After injury, astrocytes respond to the lesion, becoming hypertrophic. Activated astrocytes and
393 their paracrine response contribute to scar formation, limiting regeneration of the surviving
394 axons and their functional activity. To demonstrate an effect of the NG_Roli treatment on the
395 response of these cells, we quantified GFAP staining by a stereological approach. There was a
396 significant reduction of hypertrophic astrocytes in NG_Roli treated mice compared to untreated
397 mice in the injured spinal cord (Fig.8 B, b,c,d), as demonstrated by quantitative assessment of
398 the GFAP staining (Fig.8 B, d). The neuronal preservation and the reduced activation of
399 astrocytes correlate with the improvement of motor recovery in the acute-subacute phase after
400 the damage in SCI mice. This suggests that NG_Roli acted on the pro-inflammatory event
401 orchestrated by activated astrocytes (demonstrated here *in vitro*), as well as counteracting the
402 hypertrophic response of the astrocytes following the trauma.

403

404



405

406

407 **Figure 8**

408 **Spinal cord sections stained with NeuN (neuronal marker) (A) or GFAP (astrocyte marker)**

409 **(B) of untreated injured mice (INJ) vs NG-Roli treated mice. Cartoon shows the tract of the**

410 **spinal cord investigated (A,a;B,a). Neuronal survival is showed from the injured epicenter (-**

411 **1.3/+1.5 mm) (A, d). The total number of neurons (A,b,c e) or astrocytes (B, b,c,d) in INJ mice**

412 **compared to the NG-Roli treated group showed a significant proportion of preserved neurons**

413 **and a significant reduction of hypertrophic astrocytes in treated mice. Data are mean ± SD.**

414 **Mann-Whitney test. Statistical significance: (*) $p < 0.05$. $N = 4/5$ mice/ group.**

415

416

417 **DISCUSSION**

418 The importance of the reactive glial cells during the progression of SCI has been recently
419 recognized, but alternative approaches to reduce their pro-inflammatory response, preserving
420 more tissue and neuronal connections after the primary injury, remain a challenge. Our group
421 developed and characterized a selective controlled pharmacologic delivery system for activated
422 astrocytes in the spinal cord based on NP polymers. We tested the selectivity of a nanovector
423 towards the astrocytic component *in vitro* and *in vivo*, and demonstrated its ability to
424 pharmacologically modulate the proinflammatory response of astrocytes after the primary
425 injury. *In vitro* experiments indicated that of a larger amount of nanovectors were internalized
426 into the pro-inflammatory astrocytes compared to A2 stimulated astrocytes. The internalization
427 was mediated by a clathrin-dependent endocytotic pathway, as demonstrated by inhibition after
428 CPZ treatment. Smaller amounts of NG were detected in LPS stimulated microglia, even less
429 in M2 stimulated microglia, and no one in neurons.

430 After internalization into the cytoplasm of astrocytes, NG undergoes lysosomal degradation
431 releasing the compounds loaded into it (To-pro3 or Rolipram), demonstrating its capacity for
432 internalization, degradation and pharmacological release *in vitro*. Although NG were detected
433 in microglia the amount found was very small, and it seems that the mechanisms of
434 internalization and degradation were different than for astrocytes. NG was not addressed to the
435 lysosome for degradation once internalized in the microglia.

436 Many types of cells use the clathrin- and caveolae-mediated endocytosis pathways to
437 internalize nanoscale materials.^{20,21} These endocytic pathways are the most important ones for
438 the internalization of NP and clathrin-mediated endocytosis with lysosome-oriented
439 degradation was also seen here for astrocytes. The lack of colocalization with lysosomes in
440 microglia suggests alternative uptake mechanisms for NG, such as caveolae-mediated

441 endocytosis pathways, which avoid lysosomal degradation or clathrin- and caveolae-
442 independent endocytosis.²⁰

443 Microglia also internalize NG differently from other nanovectors previously tested in our
444 group, such as PCL-based NPs that were taken up by clathrin-dependent endocytosis and
445 degraded by lysosomes by the microglia.^{18,22} These experiments showed a limited uptake for
446 NG compared to the amount of PCL internalized in activated microglia.

447 Human iPS cells lend themselves to many applications, but to our knowledge no studies have
448 reported their use to evaluate the delivery ability of nanovectors. We demonstrate that NG, as
449 formulated here, were internalized and degraded in iPS human-derived astrocytes, as
450 demonstrated in murine astrocytes, suggesting potential translability to the clinic.

451 We also demonstrated *in vivo* and *ex vivo* the validity of NG as a nanovector, whose
452 internalization occurred almost exclusively on astrocytes in the SCI mouse model. Some
453 microglia in the injured site showed a few internalized NG, but very few compared to
454 astrocytes, quite likely because of the effects on the membrane of these cells in the more
455 damaged part of the spinal cord.

456 The ability of this tool to deliver compounds was further evaluated *in vitro* and *in vivo*, and an
457 anti-inflammatory drug (Rolipram) when administered by NG modulated the response of the
458 astrocytic component by reducing the production of specific inflammatory molecules such as
459 iNOS and Lcn2. CM collected from microglia treated with Rolipram-loaded NG did not
460 influence motor neuron survival. Thus, we can consider the amount of NG internalized into the
461 microglia irrelevant for the treatment.

462 We also demonstrated that reducing the paracrine inflammatory response of activated
463 astrocytes by Rolipram-loaded NG reversed motor neuron toxicity *in vitro*. The neuroprotective
464 effect was detected in the acute-subacute phase after the lesion and confirmed by motor
465 functional improvement from 7 to 21 DPI. NG treatment alone also served to partially regain

466 motor control at 21 DPI. NG treatment *in vivo* suggests an effect on astrocytes due to the
467 polymeric structure, but this requires further study. We also showed *ex vivo* that Rolipram-
468 loaded NG preserved neurons and reduced astrocytes at 14 DPI; these neurons were not
469 preserved at 63 DPI, supporting the behavioral findings.

470 The post-injury astrocyte response is recognized an important contributor to functional
471 recovery after traumatic SCI.^{23,24} Recent studies have made important progress in astrogliosis
472 after CNS injuries, identifying specific roles and marker genes for different astrocyte subtypes.
473^{3,23-25} Astrocytes activated by molecular mediators released in the environment, acting as pro-
474 inflammatory or anti-inflammatory stimuli³, in turn play an important role in the inflammatory
475 response.³ Reactive astrocytes after activation increase GFAP^{1,2,26} and release many molecules.
476 One of them, Lcn2, can promote neuronal death^{27,28} and acts as an inflammatory molecule
477 contributing to the secondary injury damage in SCI.²⁷ In the chronic phase, the reactive
478 astrogliosis lead to extracellular matrix deposition and formation of glial scar.^{1,26}

479 Here we demonstrated that a nanovector tool such as NG can treat pharmacologically activated
480 astrocytes with an anti-inflammatory drug (Rolipram), to reduce the amount of Lcn2 and iNOS
481 produced by these cells. The secretion of Lcn2 and iNOS contributes to inflammation in many
482 CNS pathologies, including SCI.^{27,29} iNOS produces a large amount of NO that causes
483 pathological changes in various biological substrates (peroxidation of the cellular lipid
484 components), resulting in cellular damage.²⁹ Lcn2 secreted by astrocytes further sustains
485 inflammation which in turn promotes neuron death.^{27,28,30} Lcn2 is activated by signaling
486 pathways such as NF-kB or STAT3.³¹⁻³³ We found that Rolipram acted on NF-kB to reduce
487 the mRNA levels of Lcn2 and concomitantly iNOS, potentially limiting the negative effect of
488 a pro-inflammatory response of astrocytes. Deletion of Lcn2 limits the pro-inflammatory
489 phenotypes of activated astrocytes *in vitro* and *in vivo*^{30,34}, giving greater recovery in mouse
490 models of SCI.²⁷ Lcn2 knock-out mice had consistent neuronal survival and myelin sparing

491 after SCI.²⁷ Acting on iNOS and Lcn2 looks like a promising therapeutic approach that could
492 be associated to other treatments to strengthen the effect.

493

494 **CONCLUSION**

495 Different nanovectors are internalized into astrocytes, but none in a selective way for treating
496 the astroglial pro-inflammatory response.³⁵ Because astrogliosis is closely interlaced and
497 dynamic depending on the injury phase, it may have beneficial or detrimental effects on SCI
498 recovery. It is important therefore to develop strategies to target individual cellular and
499 molecular mechanisms. This study demonstrated the selective efficacy of Rolipram delivered
500 by biodegradable NG in limiting the pro-inflammatory response mediated by astrocyte
501 activation in a mouse model of SCI, but other diseases with an astrocyte-based glial response
502 may gain too from this selective therapeutic approach. This delivery strategy could also be
503 considered for **other molecules able** to promote neuroprotective astrocytes (A2 phenotype),
504 opening the way to a new cell-specific therapeutic treatment to ameliorate SCI and other
505 neurological diseases.

506

507 MATERIALS AND METHODS

508

509 *NANO GEL DESIGN AND CHARACTERIZATION*

510 The experimental procedures required the following polymers in the nanogel (NG) design:
511 polyethylene glycol 8000 (Mw 8 kDa, from Merck KGaA, Darmstadt, Germany) and linear
512 polyethyleneimine 2500 (Mw 2.5 kDa, from Polysciences Inc., Warrington, USA). All other
513 chemicals were purchased from Merck (Merck KGaA, Darmstadt, Germany) and used as
514 received, without any further purification. Solvents were of analytical-grade purity. All the Cy-
515 5 derivatives were stored at -20°C.

516 NG was synthesized according to this procedure: PEG hydroxyl groups were modified with
517 imidazole moieties and PEI functionalized with Cy5 (molar ratio PEI: Cy5 1:0.025) using
518 copper-catalyzed azide-alkyne Huisgen cycloaddition (CuAAC) reaction. Then two solutions
519 were prepared separately: in the first, the resulting PEG (200 mg, 0.025 mmol) was dissolved
520 in CH₂Cl₂ (3 mL), and the second one was obtained by dissolving PEI conjugated Cy5 (52 mg,
521 0.017 mmol) in distilled water (5 mL). The organic solution was added dropwise to the aqueous
522 system, under vigorous stirring, and the final mixture was sonicated for 30 min. The polymeric
523 mixture was then stirred for 17 h at 25°C (room temperature, r.t.) with the gradual evaporation
524 of CH₂Cl₂. This aqueous system was purified by dialysis against slightly acid water and
525 lyophilized, resulting in a green solid.

526 The primary amines were grafted around the NG surface. NG (15 mg, 0.566 mol) were
527 dissolved in distilled water (1 mL) and kept under stirring at r.t. 3-bromopropylamine
528 hydrobromide, the chemical carrying -NH₂ groups, (4.95 mg, 22.64 μmol) was dissolved in
529 distilled water (0.5 mL) and added dropwise to the NG solution. The mixture was stirred for
530 17h, in the dark, at r.t.

531 Dialysis against distilled water (1000 mL) using a regenerated cellulose membrane (MW cut-
532 off 6-8 kDa) was done for two days, with daily water exchange, to remove unreacted species
533 and any by-products. The system was frozen at -80°C and the product was recovered by
534 lyophilization. These NG coated with primary amine moieties will be indicated as NG.
535 Polymer functionalizations were evaluated by NMR and FT-IR analyses. ^1H -NMR spectra
536 were run on a Bruker AC (400 MHz) spectrometer, using deuterated chloroform (CDCl_3) for
537 PEG and NG samples, and deuterium oxide (D_2O) for PEI derivatives as solvents, and chemical
538 shifts were reported as δ values in parts per million, tetramethylsilane (TMS) as internal
539 reference. FT-IR spectra were recorded using the KBr pellet technique for the analyzed samples
540 and a Thermo Nexus 6700 spectrometer coupled to a Thermo Nicolet Continuum microscope
541 equipped with a $15\times$ Replachromat Cassegrain objective, at r.t. in air in the wave range 4000--
542 500 cm^{-1} , with 64 accumulated scans and a resolution of 4 cm^{-1} . The nanogel size,
543 polydispersity index (PDI) and z-potential were recorded using Dynamic Light Scattering
544 (DLS) and a Zetasizer Nano ZS from Malvern Instruments. The samples were dissolved in
545 distilled water and the solution was equilibrated for 60 s before data analysis at 37°C . Data are
546 the mean of three measurements for each NG. NG dimensions were studied with Atomic Force
547 Microscopy (AFM). The samples were prepared by dropping nanogel latexes onto silicon
548 substrate and then drying. AFM images on $1 \times 1\ \mu\text{m}$ areas were recorded for the preliminary
549 morphologic evaluation; $500 \times 500\text{ nm}$ images were cropped and a height line profile was
550 drawn for each single gel. Surface morphology was evaluated by flattening the images (first
551 order) using NTMDT software.

552

553 *PRIMARY CELL CULTURES*

554 Primary cultures of microglia, astrocytes, or astrocyte/neuron co-cultures were obtained from
555 the spinal cord of 13-days-old C57BL/6J mouse embryos (Charles River Laboratories
556 International, Inc.) by adapting protocols previously described ³⁶.

557 Ventral horns were isolated from the embryonic spinal cord and treated with DNase and trypsin
558 (Sigma-Aldrich). After centrifugation using a cushion of bovine serum albumin (BSA), a mixed
559 population of neurons/glia was obtained. A second centrifugation (800 x g for 15 min) was
560 done through a 6% iodixanol pillow (OptiPrep™; Sigma-Aldrich). At the top of the iodixanol
561 pillow a narrow band was obtained, corresponding to the fraction enriched with motoneurons,
562 and a yellow pellet. The glial feeder layer was prepared by plating the glial fraction at a density
563 of 25,000 cells/cm² in flasks pre-coated with poly L-lysine (Sigma-Aldrich).

564 From the flask containing confluent mixed glial cultures, purified microglia were obtained after
565 shaking at 275 rpm overnight in incubators. The floating cells (mostly microglia) were collected
566 and seeded at a density of 40,000 cells/cm² on poly-L-lysine pre-coated 24-well plates.

567 To obtain astrocyte-enriched cultures, glial cultures from which the microglia had previously
568 been collected were treated with 60 mM L-leucine methyl ester (Sigma-Aldrich) for 90
569 minutes. To derive purified cultures and to establish a glial feeder layer for neuron/astrocyte
570 co-cultures, the astrocytes were collected and seeded at a density of 40,000 cells/cm² on 24-
571 well plates pre-coated with poly-L-lysine.

572 Finally, to establish neuron/astrocyte co-cultures, the motor neuron-enriched fraction (from the
573 iodixanol-based separation) was seeded at a density of 15,000 cells/cm² onto a mature astrocyte
574 layer. In these co-cultures, about 84±5% of the neurons were SMI32-positive, with the typical
575 motor neuron morphology, as previously reported. ³⁶

576

577 *IPSc-DERIVED ASTROCYTE CULTURES*

578 Episomal human iPSC (hiPSC) were obtained from Gibco™ (Life Technologies, CA, US, Lot
579 V2.0). The hiPSC line was cultured and expanded in feeder-free conditions by passaging every
580 3–5 days when they reached 70–80% confluence in a xeno-free culture medium formulation
581 (StemMACS™ iPS-Brew XF, Miltenyi Biotec S.r.l.). Neural stem cells (NSC) were derived
582 from hiPSC using a commercial manufactured culture medium in a monolayer protocol ³⁷.
583 Briefly, hiPSCs cultured in feeder-free conditions were split into six-well plates in a 1:3 ratio.
584 The day after plating, culture medium was replaced with Gibco PSC Neural Induction Medium
585 (Life Technologies) containing Neurobasal medium and Gibco PSC neural induction
586 supplement. On day seven of neural induction, primitive NSCs (pNSCs) were dissociated with
587 Accutase (Life Technologies), passed through a 100-µm strainer and plated on Geltrex-coated
588 dishes at a density of 0.5–1x10⁵ cells/cm² in an NSC expansion medium, composed Neurobasal
589 medium and Advanced DMEM/F12 (1:1), with 2% neural induction supplement. NSC were
590 expanded for different passages before the induction of astrocyte differentiation.

591 To obtain differentiated astrocyte cultures, dissociated pNSCs in the sixth through the tenth
592 passage (P6-10) were plated onto Geltrex-coated 24-well plates at a density of 5x10⁴ cells/cm²
593 in an astrocyte differentiation medium (DMEM supplemented with 1% N2, Glutamax and fetal
594 bovine serum (FBS); Life Technologies) for twenty-one days.

595 On the day twenty-one of astrocyte differentiation, cultures were exposed to LPS (10 µg/mL)
596 for 18h or A1 phenotype was induced by treatment with FGF (100 ng/mL) for 18h in medium
597 with 10% serum. Empty NG was then added to activate cultures and time-lapse analysis was
598 done for up to three days to establish the degradation time of NG. To assess the NG degradation
599 by lysosomes, human astrocytes were marked with Lyso sensor dye (1:20.000 dilution, Life
600 Technologies, cat. n. L7535) 24h after exposure. Culture samples were processed in parallel to
601 verify the expression of astrocyte markers and the absence of stem cells.

602

603 *CULTURE TREATMENTS*

604 Microglia activation was induced by exposing purified microglia cultures to 1 µg/mL of LPS
605 (from *Escherichia coli* 0111:B4; Sigma-Aldrich), as previously reported³⁶, or IL-4 10 ng/mL
606 for 18h. The murine astrocytes was activate by LPS 1 µg/mL, A1 phenotype was induced by
607 treatment with C1q 400 ng/mL, TNFα 30 ng/mL, IL1α 3 ng/mL for 24h³ and A2 phenotype
608 was induced by treatment with FGF (100 ng/mL) for 18h. Empty NG, NG loaded with Rolipram
609 loaded with To-pro3, or free Rolipram, were then added to the activated cultures. To investigate
610 NG uptake, we treated astrocytes with chlorpromazine hydrochloride (CPZ; Sigma-Aldrich),
611 CPZ (40 µM) 2h before NG exposure.

612 Astrocyte/neuron co-cultures were treated with CM from microglia or astrocytes incubated
613 with different treatments for 24h: after microglial activation, cells were incubated with fresh
614 medium or NG or NG loaded with Rolipram for 24h, while astrocytes were induced toward A1
615 and treated with NG or NG loaded with Rolipram for 24h. At the end of the treatment, motor
616 neuron cultures were stained with SMI-32 antibody (Biolegend; 1:1000) and stereologically
617 counted (see below).

618

619 *NG INTERNALIZATION*

620 To quantify the internalization of NG in murine and human cells, images were randomly
621 selected and acquired 24h, three and five days after the NG exposure with a Cell R microscope
622 (Olympus) equipped with 60X magnification and an ORCA camera (Hamamatsu).

623 The fluorescent signal was quantified using the free Fiji software (<http://fiji.sc/Downloads>).

624 The NG signals in single cells (about 30-50) were evaluated as the ratio between the Cy5 signal
625 area and the cell area. To overcome the limits associated with a change of the shape seen after
626 treatment with FGF (for in vitro astrocytes) or IL-4 (for in vitro microglia) we investigated the

627 NG signal for single cells (region of interest determined by fluorescein staining) for comparing
628 these treatments.

629

630 *REAL TIME RT-PCR*

631 Total RNA was extracted from astrocytes or microglial cultures using a miRNeasy Mini Kit
632 (Qiagen, Valencia, CA, USA). Briefly, cells were collected in QIAzol Lysis Reagent and lysed
633 with a pipette. Chloroform was added to the homogenate and a phase extraction was done. A
634 small volume of the aqueous phase (0.3 mL) was added to 450 mL of ethanol and loaded onto
635 an RNeasy column. The column was washed and RNA eluted following the manufacturer's
636 recommendations. RNA was quantified by a spectrophotometer at 260 nm for all samples. To
637 remove any contaminating genomic DNA, total RNA was digested with DNase (Applied
638 Biosystems) and reverse-transcribed with random hexamer primers using Multi-Scribe Reverse
639 Transcriptase (Taq-Man Reverse transcription reagents; Applied Biosystems). Realtime RT-
640 PCR was run using 4 uL of cDNA, 200 nmol of each primer and SYBR Green chemistry
641 (Applied Biosystems) in a total volume of 22 uL. After completion of qPCR, a melting curve
642 of amplified products was plotted. Data were collected using the SYBR Green fluorescence
643 during Real-Time RT-PCR on an Applied Biosystems 7300 system. The expression of the
644 following genes was analyzed:

645 iNOS (Fw: GACGAGACGGATAGGCAGAG; Rev: GTGGGGTTGTTGCTGAACTT)

646 Lcn2 (Fw: TTTGTTCCAAGCTCCAGGGC; Rev: TGGCGAACTGGTTGTAGTCC)

647 β -Actin (Fw: CGCGAGCACAGCTTCTTT; Rev: GCAGCGATATCGTCATCCAT)

648 β -Actin was used as the reference gene and relative expression levels were evaluated according
649 to the manufacturer's DDCT method (Applied Biosystems). Data are expressed as the fold
650 change from uninjured spinal cord (healthy condition).

651

652 *IMMUNOCYTOCHEMISTRY*

653 Motor neurons were fixed with 4% paraformaldehyde for 40 min then incubated for 1h at r.t.
654 in the blocking solution (PBS, 0.2% Triton X-100 (Sigma-Aldrich) and 1% FBS (Sigma
655 Aldrich). Anti-SMI-32 primary antibody (mouse; BioLegend) was diluted (1:1000) in PBS and
656 incubated at r.t. for 4h. The sections were washed with PBS and the appropriate fluorescent
657 secondary antibody was diluted in PBS and incubated for 1h at r.t.

658

659 **CELL STAINING**

660 Cells were fixed with 4% paraformaldehyde for 40 min and stained with Fluorescein (0.1
661 ug/mL; Sigma-Aldrich) for 30 min at r.t. For evaluation of live cells, they were incubated with
662 CellTrace™ CFSE Cell proliferation kit (1:1000 dilution, Life Technologies, cat n.C34554)
663 for 30 min. To measure lysosomal activity we used lysosensor dye (1:20.000 dilution, Life
664 Technologies, cat. n. L7535). Cell nuclei were labeled with Hoechst 33258 (Invitrogen) by
665 incubation with a 250 ng/mL solution.

666

667

668 *NUMBER OF MOTOR NEURONS IN VITRO*

669 Images of the entire wells were acquired with a Cell R microscope (Olympus) equipped with
670 an ORCA camera (Hamamatsu) using a mosaic imaging protocol with 20X magnification. For
671 frame sampling a grid (1000*1000 μ m single frame) was superimposed on the images and
672 alternate frames were examined with stereological probes (unbiased fractionator probe
673 dimension, 307*235 μ m). The total number of motor neurons was calculated with the following
674 formula: $N = \sum Q * 1/asf * 1/ssf$, where Q was the number of neurons counted in the frame, the
675 area probe 307*235 μ m, the area frame 1000*1000 μ m, asf (area probe/area frame), and ssf
676 (sampling fraction of every 2nd frame). Intra-animal coefficient of error (CE) and inter-animal

677 coefficient of variation (CV) for neuronal counts^{38,39} were calculated as follows: mean CE for
678 co-culture motor neurons/astrocytes treated with PI and astrocyte conditioned medium: CTR-
679 CM 0.082, PI 0.080, PI-NG 0.058, PI-NG-Roli 0.071. CV: CTR-CM 0.243, PI 0.126, PI-NG
680 0.343, PI-NG-Roli 0.197. Mean CE for co-culture motor neurons/astrocytes treated with PI and
681 microglia conditioned medium: CTR-CM 0.075, PI 0.068, PI-NG 0.075, PI-NG-Roli 0.073 and
682 CV: CTR-CM 0.178, PI 0.216, PI-NG 0.197, PI-NG Roli 0.300.

683

684 *ANIMAL CARE*

685 The IRCCS adheres to the principles set out in the following laws, regulations, and policies
686 governing the care and use of laboratory animals: Italian Governing Law (D.lgs 26/2014;
687 Authorisation n.19/2008-A issued March 6, 2008 by Ministry of Health); Mario Negri
688 Institutional Regulations and Policies providing internal authorization for persons conducting
689 animal experiments (Quality Management System Certificate – UNI EN ISO 9001:2015 – Reg.
690 N° 6121); the NIH Guide for the Care and Use of Laboratory Animals (2011 edition) and EU
691 directives and guidelines (EEC Council Directive 2010/63/UE). The Statement of Compliance
692 (Assurance) with the Public Health Service (PHS) Policy on Human Care and Use of
693 Laboratory Animals was been recently reviewed (9/9/2014) and will expire on September 30,
694 2019 (Animal Welfare Assurance #A5023-01).

695

696 *SURGERY*

697 C57BL/6J mice (Charles River Laboratories International, Inc.) or B6.129P-Cx3cr1tm1Litt/J
698 mice (The Jackson Laboratory) were used for *in vivo* studies. Before surgery, the animals
699 received an antibiotic and analgesic, with respectively subcutaneous injection of ampicillin (50
700 mg/kg) and buprenorphine (0.15 mg/kg). The entire surgical procedure was carried out in deep
701 anesthesia under ketamine hydrochloride (IMALGENE, 100 mg/kg) and medetomidine

702 hydrochloride (DOMITOR, 1 mg/kg) intraperitoneally. Animals were placed on a Cunningham
703 Spinal Cord Adaptor (Stoelting, Dublin, Ireland) mounted on a stereotaxic frame, and
704 laminectomy of the T12 vertebra was done to uncover the lumbar spinal cord. Mechanical
705 trauma of the spinal cord at T12 was induced using an [Mann-Whitney test](#) with a closing force
706 of 30g (left in place for 1 min, then removed). After spinal cord compression, dorsal muscles
707 were juxtaposed using absorbable sutures and the skin was sutured. Two hours (for NG
708 distribution experiment) or one day (for behavioral evaluation) after surgery, the spinal cord of
709 SCI mice was exposed and injected intraparenchymally with NG, NG-Cy5 loaded with
710 Rolipram or free Rolipram. Six 0.250 uL injections were done with a glass capillary ([outer](#)
711 [diameter 40±2 μm](#)), to cover the injured area. The capillary was positioned ±0.5 mm from the
712 midline, then it was deepened into the parenchyma to 0.6 mm below the pia mater. After
713 treatment, dorsal muscles were juxtaposed using absorbable sutures and the skin was sutured
714 and disinfected.

715

716 *BEHAVIORAL EVALUATIONS*

717 Mice after SCI were evaluated by testing hind-limb locomotor performances using the Basso
718 Mouse Scale (BMS) once a week from seven to thirty-five DPI. The BMS is a 10- point scale
719 (9 = normal locomotion; 0 = complete hind limb paralysis). Video acquisition of the locomotor
720 performances (5 min) was done with camera (Denver, ACG-8050W) and evaluated by two
721 independent observers, blinded to the treatment. Individual hind-limb scores were averaged for
722 each animal group at each time point.

723

724 *SPINAL CORD TRANSCARDIAL PERFUSION*

725 For histological analysis, under deep anesthesia with ketamine hydrochloride (IMALGENE,
726 100 mg/kg) and medetomidine hydrochloride (DOMITOR, 1 mg/kg), the mice were

727 transcardially perfused with 40 mL of phosphate buffer saline (PBS) 0.1 mol/L, pH 7.4 for 4
728 min, followed by 50 mL of paraformaldehyde solution (4%) in PBS for 5 min. Spinal cords
729 were carefully removed and post-fixed overnight in the same fixative at 4°C, then transferred
730 to 30% sucrose in 0.1 mol/L phosphate buffer overnight for cryopreservation and stored at 4°C
731 until use.

732

733 *IMMUNOFLUORESCENCE*

734 The spinal cord was embedded in OCT compound, frozen by immersion in N-pentane at -45°C
735 for 3 minutes, then stored at -80°C until use. Frozen tissues were sectioned at 30 μm using a
736 cryostat at -20°C, starting from the rostral edge (about 6 mm rostral to the epicenter), collected
737 in PBS and stored at 4°C until use. Twenty μm thick serial sections (one section every five)
738 were separated and immunofluorescence was done. Sections were incubated with primary
739 antibodies directed against astrocytes (Glial Fibrillary Acidic Protein (GFAP); 1:500 dilution,
740 Millipore) or neurons (NeuN, 1:500 dilution, Millipore) dissolved in PBS, 1% normal goat
741 serum (NGS; Sigma Aldrich) and 0.1% Triton X-100 and incubated overnight at 4°C under
742 constant shaking. Primary antibody staining was detected using secondary antibodies
743 conjugated to fluorophores (Alexa Fluor 647, 1:500; Invitrogen). Spinal cord sections were
744 coverslipped with a 50% glycerol solution in PBS before acquisition at 10X magnification by
745 confocal microscopy (Olympus Fv1000, Laser 594).

746

747 *COLOCALIZATION STUDY*

748 Study of colocalization was carried out *in vitro* (9-19 cells) and *ex vivo* around the site of
749 injection 1 day post-injury (9 sections, 30 μm thickness, sampled one every two sections,
750 evaluated area 5355 μm^2). Colocalization was quantified by Pearson's coefficient (Imaris
751 software, Bitplane).

752

753 *TOTAL NUMBER OF NEURONS IN DAMAGED SPINAL CORD*

754 Acquisition was set using a Cell R microscope (Olympus); Every 5th section (30 μm thickness)
755 in a tract of spinal cord of +1.5/-1.3 mm from the injury site was acquired using a 3D mosaic
756 imaging technique with 40x magnification. For frame sampling a grid (200*200 μm) was
757 superimposed on the acquired section and all frames of the grid containing grey matter were
758 examined in a fractioned height of 5 μm . An unbiased counting probe (216*165 μm) was used
759 to count neurons in each frame, with Image j software and a homemade plugin-macro. The total
760 number of neurons was calculated using the formula: $N = \sum Q * t/h * 1/asf * 1/ssf$, where Q is the
761 number of neurons counted in the section, t (section thickness, 30 μm), h (fractionator height,
762 5 μm), area probe (216*165 μm), area frame (200*200 μm), asf (area probe/area frame), ssf
763 (sampling fraction of every 5th section). The precision of the number of neuronal cells was
764 established by the intra-animal coefficient of error, CE and inter-animal coefficient of variation
765 CV. ^{38,39} Mean CE: INJ 0.050, NG_Roli 0.044 and CV: INJ 0.283, NG_Roli 0.122.

766

767 *ASTROCYTOSIS IN SPINAL CORD*

768 The acquisition was set using a Cell R microscope (Olympus). Every 5th section (30 μm
769 thickness) in a tract of spinal cord of +1.5/-1.3 mm from the injury site was acquired using a
770 3D mosaic imaging technique with 40x magnification. For frame sampling a grid (200*200
771 μm) was superimposed on the acquired section and all frames of the grid containing astrocytes
772 marked with GFAP were examined in a fractioned height of 2 μm . An unbiased counting probe
773 (216*165 μm) was used to quantify GFAP⁺ staining in each frame, with Image j software and
774 by the Cavalieri method. Volume was calculated as: $V = \sum P * A * T$ (V volume, P number of
775 points hitting white matter, A, grid spacing (200*200 μm) and T, distance between each

776 sampled section (150 μm). CE and CV were calculated^{38,39}: mean CE: INJ 0.067, NG_Roli
777 0.085. CV: INJ 0.265, NG_Roli 0.285.

778

779 *STATISTICAL ANALYSES*

780 We used Prism software (Graphpad) for statistical analyses. Mann-Whitney test and one-way
781 ANOVA followed by Bonferroni's post hoc test were used see relative captions.

782

783 **Acknowledgment.**

784 Authors' research is supported by Politecnico di Milano.

785

786 **Supporting Information Available:**

787 The Supporting Information is available free of charge via the Internet at <http://pubs.acs.org>

788 Scheme of NG synthesis; AFM images of NG-NH₂; FT-IR spectra of NG and NG-NH₂;

789 ¹H-NMR (D₂O) spectra of NG and NG-NH₂; NG uptake in untreated, LPS-treated and FGF-

790 IL-4 treated cell of murine astrocytes and microglia, and human astrocytes in vitro; in vitro

791 release profile of Rolipram delivered from NGs; quantitative mRNA analysis of iNOS and Lcn2

792 expressed by astrocyte cultures after treatment with three factors C1q, IL1 α and TNF, (PI) or

793 PI and Rolipram; neuron culture exposed to conditioned medium of untreated astrocytes or

794 conditioned medium of astrocytes pre-incubated for 24h with PI, PI + NG or PI+ Rolipram-

795 loaded NG; neuron culture exposed to conditioned medium of untreated microglia or

796 conditioned medium of LPS or LPS + NG or LPS +Rolipram-loaded NG pre-treated microglia;

797 number of neurons of untreated injured mice compared to Rolipram loaded NG at 63 DPI.

798

799

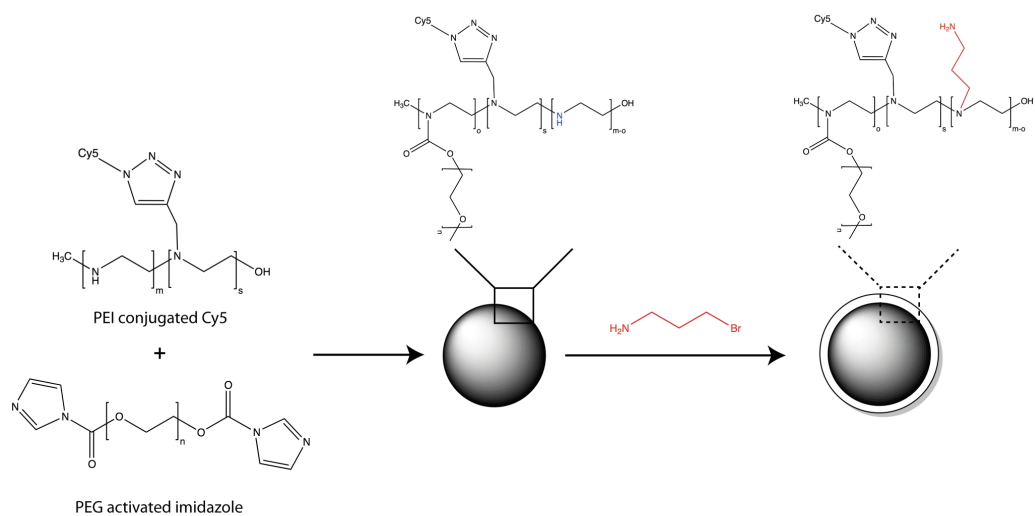
800

801

802

804 SUPPLEMENTARY

805



806

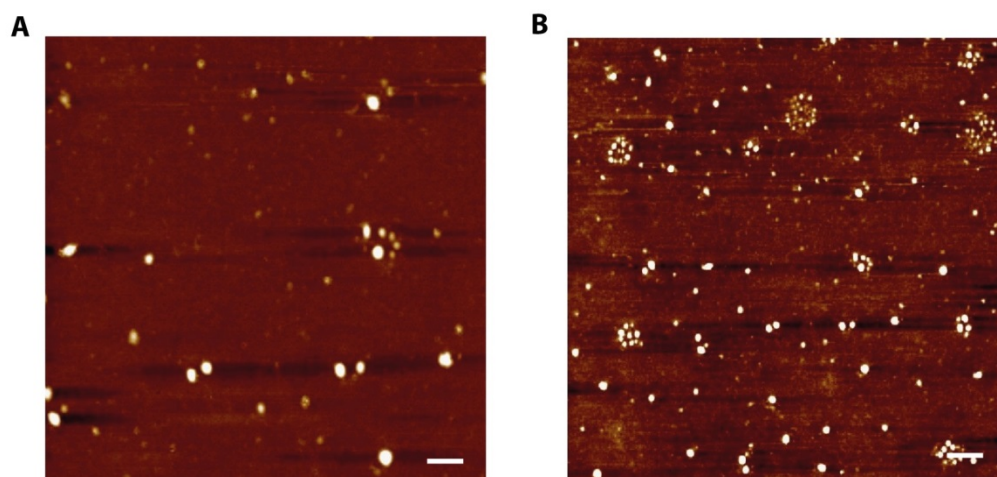
807

808 **Fig. S1**

809 *Scheme of nanogel synthesis. PEI residual amine groups are in blue, and structure of the*
810 *coating in red.*

811

812



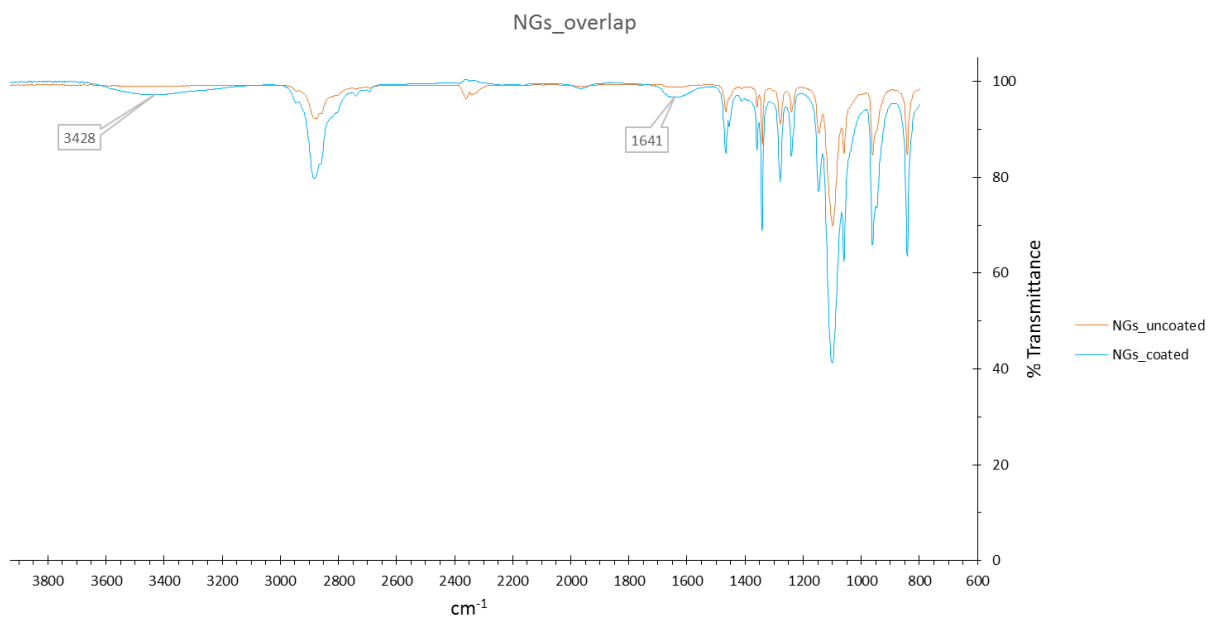
813

814

815 **Fig. S2**

816 *AFM images of NG-NH₂ (coated nanogels). Scale bars: 500 nm (A), 1000 nm (B).*

817

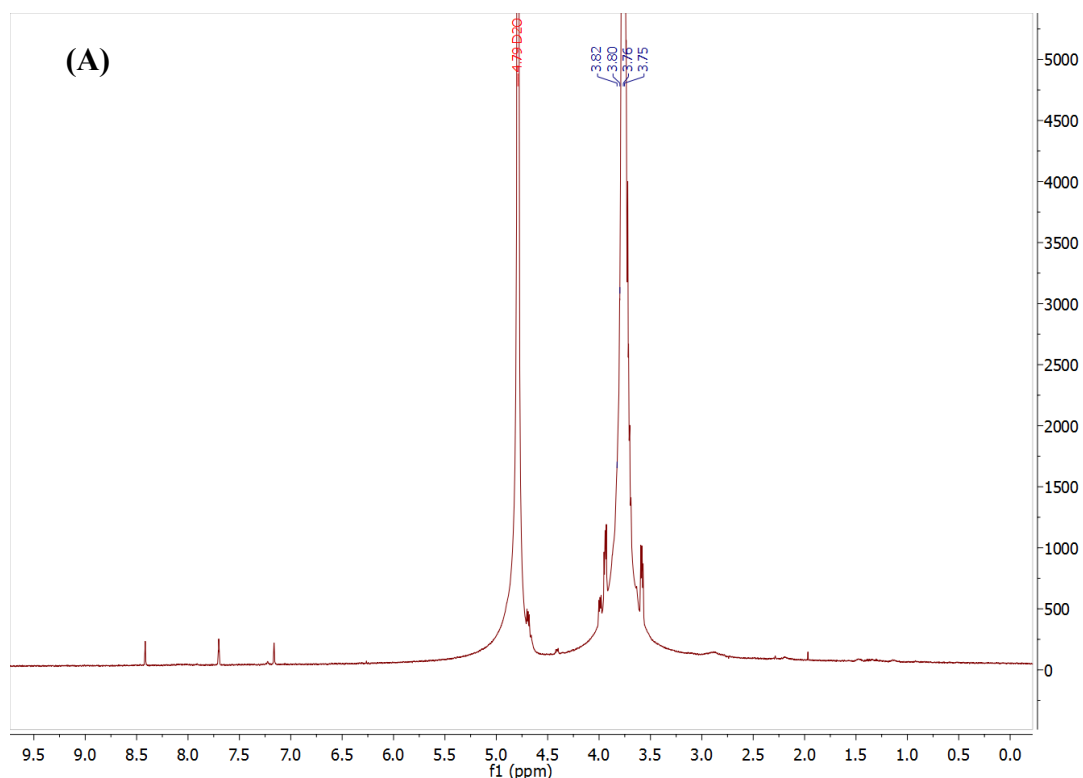


818

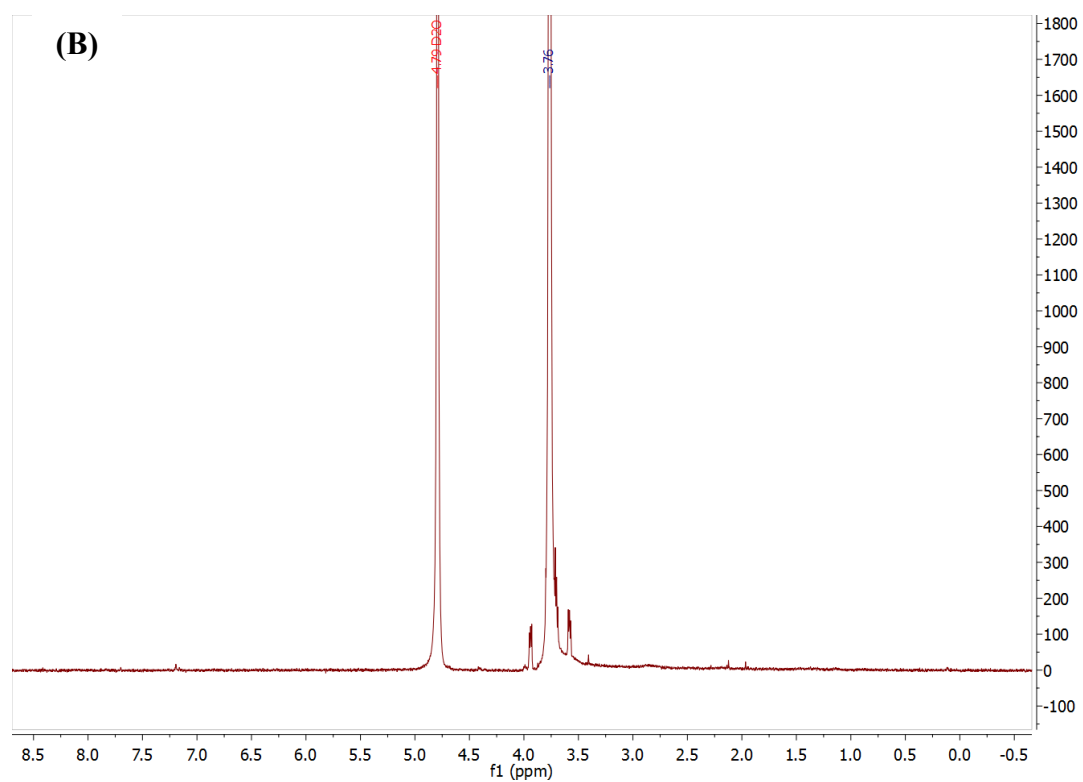
819 **Fig. S3**

820 *FT-IR spectra of NG (orange line) and NG-NH₂ (blue line).*

821



822



823

824

825 **Fig. S4**

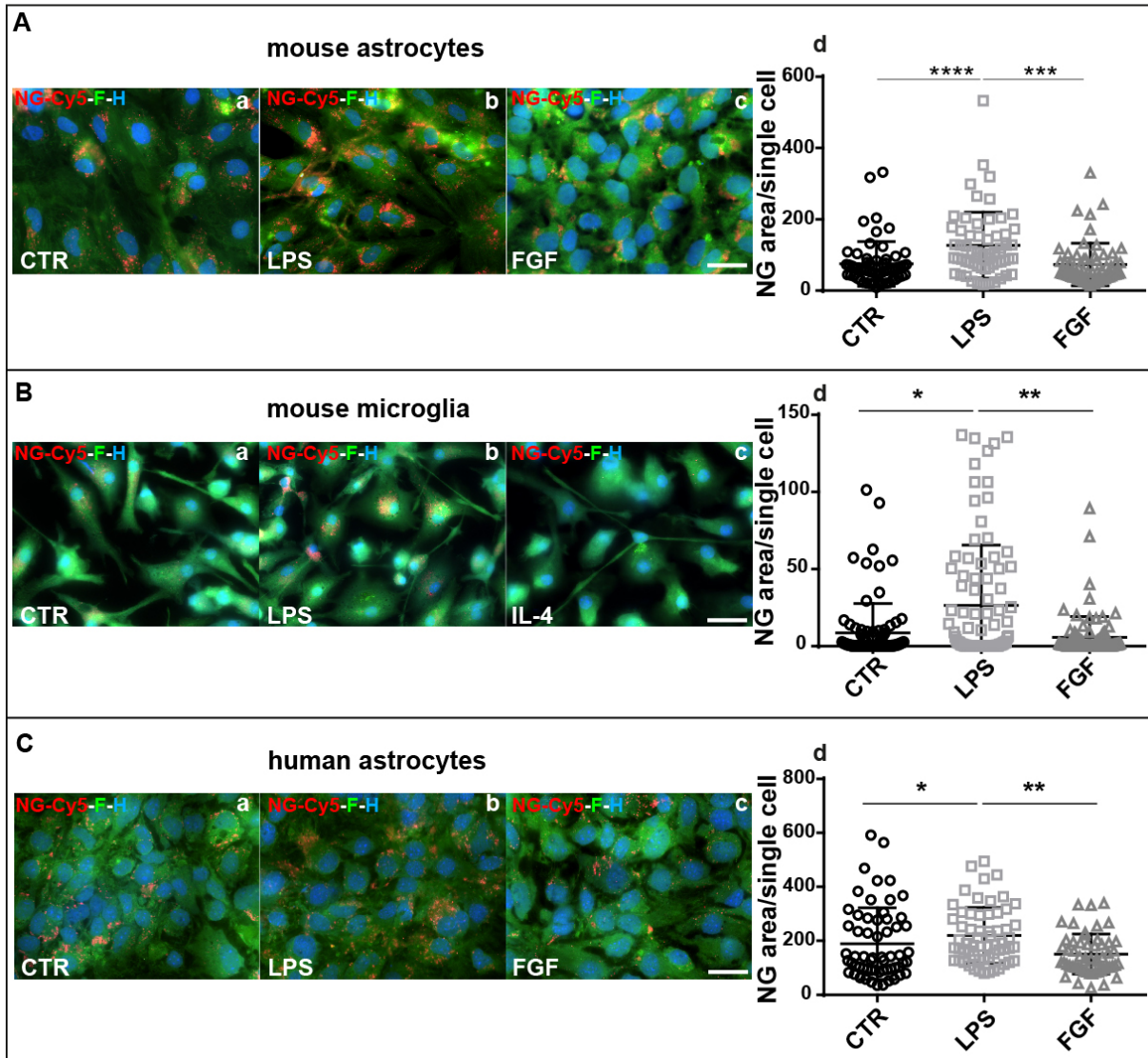
826 **$^1\text{H-NMR}$ (D_2O) spectra of NG (A) and NG-NH₂ (B).**

827

828

829

830



831

832

833 **Fig. S5**

834 **A) NG uptake in untreated (CTR) (a), LPS-treated (activation stimuli) (b) and FGF (A2 stimuli)**

835 **(c) treated murine astrocytes in vitro. Quantification of the NG uptake in astrocytes shows**

836 **higher NG internalization in LPS treated astrocytes compared to CTR and FGF group (d). B)**

837 **NG uptake in untreated (CTR) (a), LPS-treated (activation stimuli) (b) and IL-4 (M2 stimuli)**

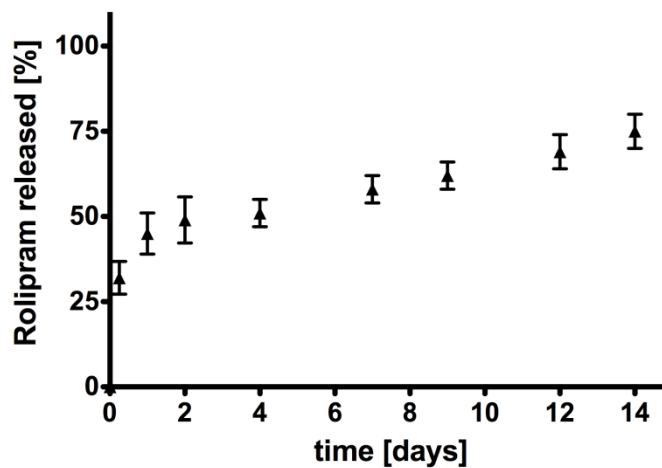
838 **(c) treated murine microglia in vitro. Quantification of the NG uptake in microglia shows**

839 higher NG internalization in LPS treated astrocytes compared to CTR and Il-4 group. C) NG
840 uptake in untreated (CTR) (a), LPS-treated (activation stimuli) (b) and FGF (A2 stimuli) (c)
841 treated human astrocytes in vitro. Quantification of the NG uptake in astrocytes shows higher
842 NG internalization in LPS treated astrocytes compared to CTR and FGF group (d). Data are
843 mean \pm SD. One-way ANOVA followed by Bonferroni's post hoc test. Statistical significance:
844 (*) $p < 0.05$, (**) $p < 0.01$, (***) $p < 0.001$, (****) $p < 0.0001$. Scale bar $10\mu\text{m}$.

845

846

847



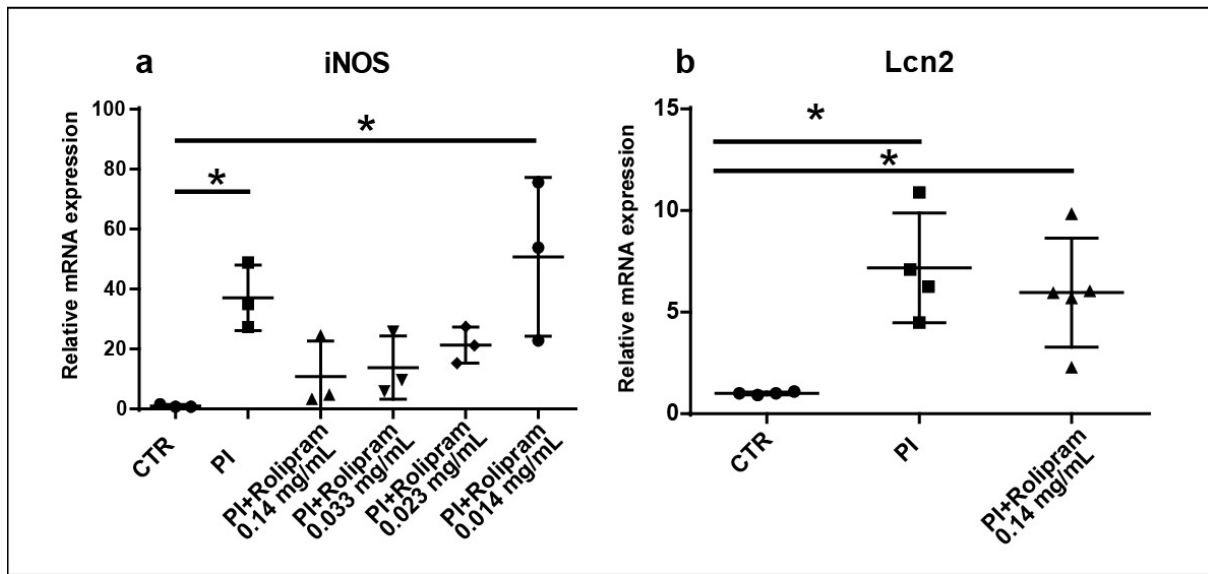
848

849 **Fig. S6**

850 *In vitro* release profile of Rolipram delivered from NGs.

851

852



853

854

855 **Fig. S7**

856 *Quantitative mRNA analysis of iNOS (a) and Lcn2 (b) expressed by astrocyte cultures after*
857 *treatment with three factors, C1q, IL1 α and TNF α (PI) or PI and Rolipram, at the*
858 *concentrations indicated. Data are mean \pm SD. One-way ANOVA followed by Bonferroni's*
859 *post hoc test. Statistical significance: (*) $p < 0.05$.*

860

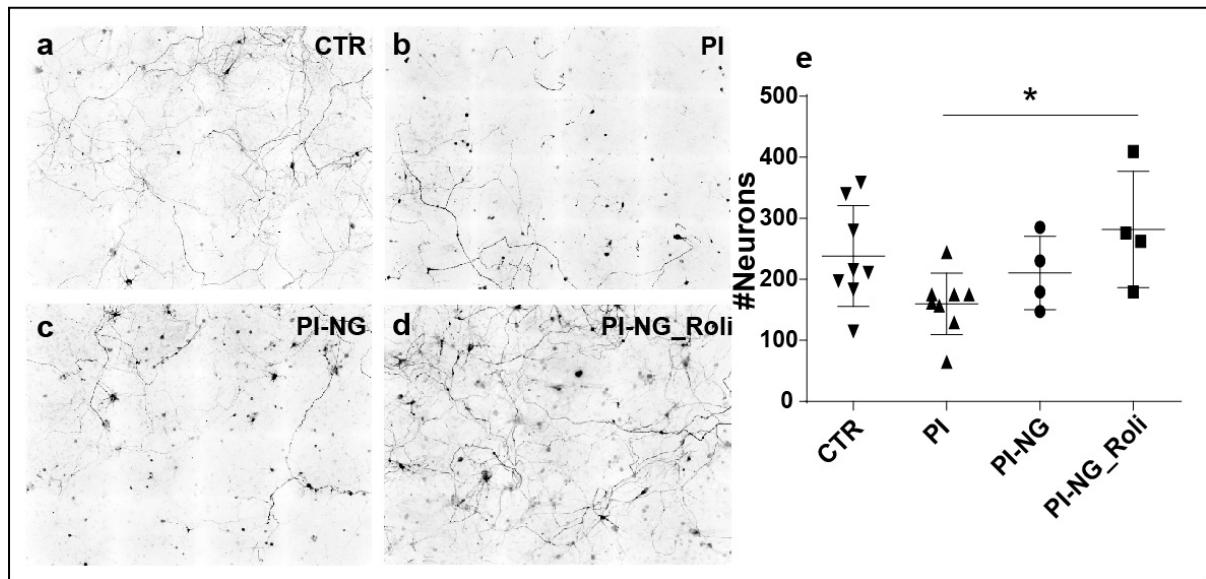
861

862

863

864

865



866

867

868 **Fig.S8**

869 *Neuron culture exposed to conditioned medium of untreated astrocytes (CTR) (a) or*

870 *conditioned medium of astrocytes pre-incubated for 24h with C1q, IL1 α and TNF α (PI) (b), PI*

871 *+ nanogel (PI-NG) (c), or PI+ Rolipram-loaded nanogel (PI-NG_Roli) (d). Cells are stained*

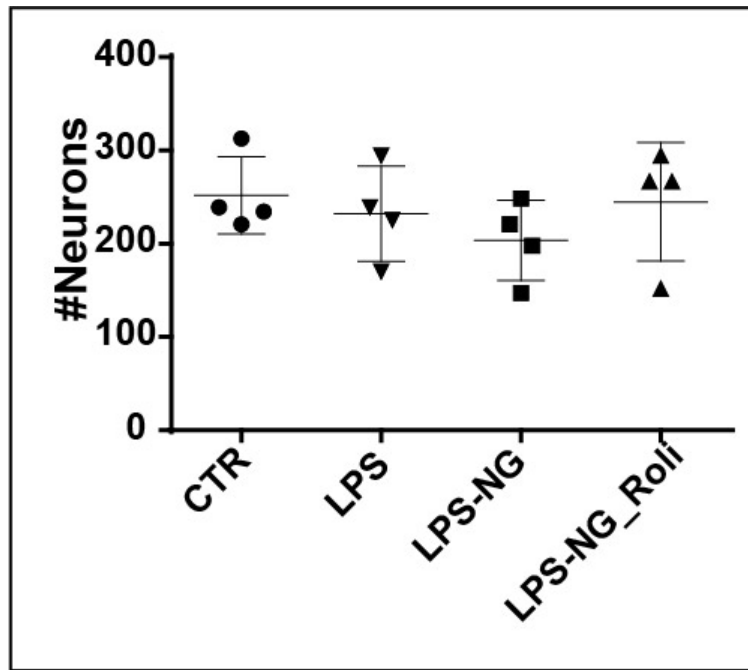
872 *for SMI32 and quantified by unbiased counting. PI-NG_Roli significantly reversed the toxicity*

873 *of the conditioned medium of PI treated astrocytes, effectively protecting motor neurons in vitro*

874 *(e). Data are mean \pm SD. One-way ANOVA followed by Bonferroni's post hoc test. Statistical*

875 *significance: (*) $p < 0.05$.*

876



877

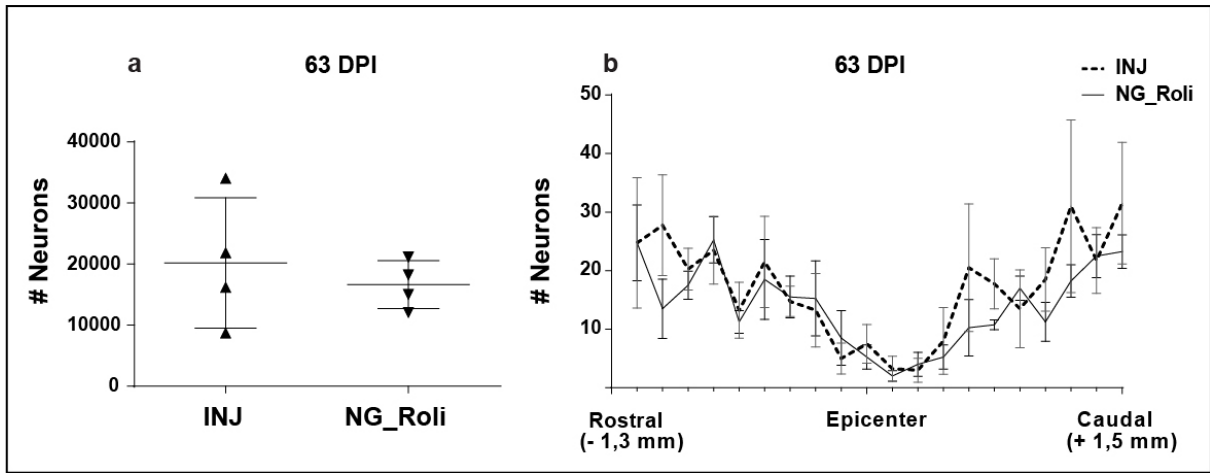
878

879 **Fig.S9**

880 *Neuron culture exposed to conditioned medium of untreated microglia (CTR) or conditioned*
 881 *medium of LPS or LPS + nanogel (LPS-NG) or LPS +Rolipram-loaded nanogel (LPS-*
 882 *NG_Roli) pre-treated microglia. Cells were stained with SMI32 and quantified by unbiased*
 883 *counting. The neuron counts show no significant differences. Data are mean \pm SD. One-way*
 884 *ANOVA followed by Bonferroni's post hoc test.*

885

886



887

888 **Fig.S10**

889 *Number of neurons of untreated injured mice (INJ) compared to Rolipram-loaded NG*
 890 *(NG_Roli) at 63 DPI. We found not significant difference between INJ and NG_Roli mice (a).*
 891 *Graphical representation of neuronal survival in relation to their distance from the injured*
 892 *epicenter at 63 DPI (b).*

893

894

895 **REFERENCES**

- 896 (1) Gaudet, A. D.; Fonken, L. K. Glial Cells Shape Pathology and Repair After Spinal Cord
897 Injury. *Neurotherapeutics : the journal of the American Society for Experimental*
898 *NeuroTherapeutics* **2018**, *15*, 554–577.
- 899 (2) Liddelow, S. A.; Barres, B. A. Reactive Astrocytes: Production, Function, and Therapeutic
900 Potential. *Immunity* **2017**, *46*, 957–967.
- 901 (3) Liddelow, S. A.; Guttenplan, K. A.; Clarke, L. E.; Bennett, F. C.; Bohlen, C. J.; Schirmer,
902 L.; Bennett, M. L.; Münch, A. E.; Chung, W.-S.; Peterson, T. C. *et al.* Neurotoxic reactive
903 astrocytes are induced by activated microglia. *Nature* **2017**, *541*, 481–487.
- 904 (4) Milich, L. M.; Ryan, C. B.; Lee, J. K. The origin, fate, and contribution of macrophages to
905 spinal cord injury pathology. *Acta neuropathologica* **2019**, *137*, 785–797.
- 906 (5) Gorshkov, K.; Aguisanda, F.; Thorne, N.; Zheng, W. Astrocytes as targets for drug
907 discovery. *Drug discovery today* **2018**, *23*, 673–680.
- 908 (6) Smith, J. A.; Braga, A.; Verheyen, J.; Basilico, S.; Bandiera, S.; Alfaro-Cervello, C.;
909 Peruzzotti-Jametti, L.; Shu, D.; Haque, F.; Guo, P. *et al.* RNA Nanotherapeutics for the
910 Amelioration of Astroglial Reactivity. *Molecular therapy. Nucleic acids* **2018**, *10*, 103–121.
- 911 (7) Bradbury, E. J.; Moon, L. D. F.; Popat, R. J.; King, V. R.; Bennett, G. S.; Patel, P. N.;
912 Fawcett, J. W.; McMahon, S. B. Chondroitinase ABC promotes functional recovery after spinal
913 cord injury. *Nature* **2002**, *416*, 636–640.
- 914 (8) Lang, B. T.; Cregg, J. M.; DePaul, M. A.; Tran, A. P.; Xu, K.; Dyck, S. M.; Madalena, K.
915 M.; Brown, B. P.; Weng, Y.-L.; Li, S. *et al.* Modulation of the proteoglycan receptor PTP σ
916 promotes recovery after spinal cord injury. *Nature* **2015**, *518*, 404–408.
- 917 (9) Siebert, J. R.; Conta Steencken, A.; Osterhout, D. J. Chondroitin sulfate proteoglycans in
918 the nervous system: Inhibitors to repair. *BioMed research international* **2014**, *2014*, 845323.
- 919 (10) Vismara, I.; Papa, S.; Rossi, F.; Forloni, G.; Veglianesse, P. Current Options for Cell
920 Therapy in Spinal Cord Injury. *Trends in molecular medicine* **2017**, *23*, 831–849.
- 921 (11) Papa, S.; Caron, I.; Rossi, F.; Veglianesse, P. Modulators of microglia: A patent review.
922 *Expert opinion on therapeutic patents* **2016**, *26*, 427–437.
- 923 (12) Caron, I.; Papa, S.; Rossi, F.; Forloni, G.; Veglianesse, P. Nanovector-mediated drug
924 delivery for spinal cord injury treatment. *Wiley interdisciplinary reviews. Nanomedicine and*
925 *nanobiotechnology* **2014**, *6*, 506–515.
- 926 (13) Rossi, F.; Perale, G.; Papa, S.; Forloni, G.; Veglianesse, P. Current options for drug
927 delivery to the spinal cord. *Expert opinion on drug delivery* **2013**, *10*, 385–396.

- 928 (14) Perale, G.; Rossi, F.; Sundstrom, E.; Bacchiega, S.; Masi, M.; Forloni, G.; Veglianese, P.
929 Hydrogels in spinal cord injury repair strategies. *ACS chemical neuroscience* **2011**, *2*, 336–345.
- 930 (15) Gao, W.; Borgens, R. B. Remote-controlled eradication of astrogliosis in spinal cord
931 injury via electromagnetically-induced dexamethasone release from "smart" nanowires.
932 *Journal of controlled release : official journal of the Controlled Release Society* **2015**, *211*, 22–
933 27.
- 934 (16) Li, X.; Kozielski, K.; Cheng, Y.-H.; Liu, H.; Zamboni, C. G.; Green, J.; Mao, H.-Q.
935 Nanoparticle-mediated conversion of primary human astrocytes into neurons and
936 oligodendrocytes. *Biomaterials science* **2016**, *4*, 1100–1112.
- 937 (17) Zhang, H.; Zhai, Y.; Wang, J.; Zhai, G. New progress and prospects: The application of
938 nanogel in drug delivery. *Materials science & engineering. C, Materials for biological*
939 *applications* **2016**, *60*, 560–568.
- 940 (18) Papa, S.; Rossi, F.; Ferrari, R.; Mariani, A.; Paola, M. de; Caron, I.; Fiordaliso, F.;
941 Bisighini, C.; Sammali, E.; Colombo, C. *et al.* Selective nanovector mediated treatment of
942 activated proinflammatory microglia/macrophages in spinal cord injury. *ACS nano* **2013**, *7*,
943 9881–9895.
- 944 (19) Papa, S.; Vismara, I.; Mariani, A.; Barilani, M.; Rimondo, S.; Paola, M. de; Panini, N.;
945 Erba, E.; Mauri, E.; Rossi, F. *et al.* Mesenchymal stem cells encapsulated into biomimetic
946 hydrogel scaffold gradually release CCL2 chemokine in situ preserving cytoarchitecture and
947 promoting functional recovery in spinal cord injury. *Journal of controlled release : official*
948 *journal of the Controlled Release Society* **2018**, *278*, 49–56.
- 949 (20) Kou, L.; Sun, J.; Zhai, Y.; He, Z. The endocytosis and intracellular fate of nanomedicines:
950 Implication for rational design. *Asian Journal of Pharmaceutical Sciences* **2013**, *8*, 1–10.
- 951 (21) Oh, N.; Park, J.-H. Endocytosis and exocytosis of nanoparticles in mammalian cells.
952 *International journal of nanomedicine* **2014**, *9 Suppl 1*, 51–63.
- 953 (22) Papa, S.; Caron, I.; Erba, E.; Panini, N.; Paola, M. de; Mariani, A.; Colombo, C.; Ferrari,
954 R.; Pozzer, D.; Zanier, E. R. *et al.* Early modulation of pro-inflammatory microglia by
955 minocycline loaded nanoparticles confers long lasting protection after spinal cord injury.
956 *Biomaterials* **2016**, *75*, 13–24.
- 957 (23) Anderson, M. A.; Burda, J. E.; Ren, Y.; Ao, Y.; O'Shea, T. M.; Kawaguchi, R.; Coppola,
958 G.; Khakh, B. S.; Deming, T. J.; Sofroniew, M. V. Astrocyte scar formation aids central nervous
959 system axon regeneration. *Nature* **2016**, *532*, 195–200.
- 960 (24) Nathan, F. M.; Li, S. Environmental cues determine the fate of astrocytes after spinal cord
961 injury. *Neural regeneration research* **2017**, *12*, 1964–1970.

- 962 (25) Zamanian, J. L.; Xu, L.; Foo, L. C.; Nouri, N.; Zhou, L.; Giffard, R. G.; Barres, B. A.
963 Genomic analysis of reactive astrogliosis. *The Journal of neuroscience : the official journal of*
964 *the Society for Neuroscience* **2012**, *32*, 6391–6410.
- 965 (26) Okada, S.; Hara, M.; Kobayakawa, K.; Matsumoto, Y.; Nakashima, Y. Astrocyte
966 reactivity and astrogliosis after spinal cord injury. *Neuroscience research* **2018**, *126*, 39–43.
- 967 (27) Rathore, K. I.; Berard, J. L.; Redensek, A.; Chierzi, S.; Lopez-Vales, R.; Santos, M.;
968 Akira, S.; David, S. Lipocalin 2 plays an immunomodulatory role and has detrimental effects
969 after spinal cord injury. *The Journal of neuroscience : the official journal of the Society for*
970 *Neuroscience* **2011**, *31*, 13412–13419.
- 971 (28) Bi, F.; Huang, C.; Tong, J.; Qiu, G.; Huang, B.; Wu, Q.; Li, F.; Xu, Z.; Bowser, R.; Xia,
972 X.-G. *et al.* Reactive astrocytes secrete lcn2 to promote neuron death. *Proceedings of the*
973 *National Academy of Sciences of the United States of America* **2013**, *110*, 4069–4074.
- 974 (29) Conti, A.; Miscusi, M.; Cardali, S.; Germanò, A.; Suzuki, H.; Cuzzocrea, S.; Tomasello,
975 F. Nitric oxide in the injured spinal cord: Synthases cross-talk, oxidative stress and
976 inflammation. *Brain research reviews* **2007**, *54*, 205–218.
- 977 (30) Jin, M.; Jang, E.; Suk, K. Lipocalin-2 Acts as a Neuroinflammation in
978 Lipopolysaccharide-injected Mice. *Experimental neurobiology* **2014**, *23*, 155–162.
- 979 (31) Lee, S.; Park, J.-Y.; Lee, W.-H.; Kim, H.; Park, H.-C.; Mori, K.; Suk, K. Lipocalin-2 is
980 an autocrine mediator of reactive astrogliosis. *The Journal of neuroscience : the official journal*
981 *of the Society for Neuroscience* **2009**, *29*, 234–249.
- 982 (32) Lee, S.; Kim, J.-H.; Kim, J.-H.; Seo, J.-W.; Han, H.-S.; Lee, W.-H.; Mori, K.; Nakao, K.;
983 Barasch, J.; Suk, K. Lipocalin-2 Is a chemokine inducer in the central nervous system: Role of
984 chemokine ligand 10 (CXCL10) in lipocalin-2-induced cell migration. *The Journal of*
985 *biological chemistry* **2011**, *286*, 43855–43870.
- 986 (33) Suk, K. Lipocalin-2 as a therapeutic target for brain injury: An astrocentric perspective.
987 *Progress in neurobiology* **2016**, *144*, 158–172.
- 988 (34) Jang, E.; Kim, J.-H.; Lee, S.; Kim, J.-H.; Seo, J.-W.; Jin, M.; Lee, M.-G.; Jang, I.-S.; Lee,
989 W.-H.; Suk, K. Phenotypic polarization of activated astrocytes: The critical role of lipocalin-2
990 in the classical inflammatory activation of astrocytes. *Journal of immunology (Baltimore, Md.*
991 *: 1950)* **2013**, *191*, 5204–5219.
- 992 (35) Zhang, F.; Lin, Y.-A.; Kannan, S.; Kannan, R. M. Targeting specific cells in the brain
993 with nanomedicines for CNS therapies. *Journal of controlled release : official journal of the*
994 *Controlled Release Society* **2016**, *240*, 212–226.

- 995 (36) Paola, M. de; Mariani, A.; Bigini, P.; Peviani, M.; Ferrara, G.; Molteni, M.; Gemma, S.;
996 Veglianesi, P.; Castellana, V.; Boldrin, V. *et al.* Neuroprotective effects of toll-like receptor
997 4 antagonism in spinal cord cultures and in a mouse model of motor neuron degeneration.
998 *Molecular medicine (Cambridge, Mass.)* **2012**, *18*, 971–981.
- 999 (37) Yan, Y.; Shin, S.; Jha, B. S.; Liu, Q.; Sheng, J.; Li, F.; Zhan, M.; Davis, J.; Bharti, K.;
1000 Zeng, X. *et al.* Efficient and rapid derivation of primitive neural stem cells and generation of
1001 brain subtype neurons from human pluripotent stem cells. *Stem cells translational medicine*
1002 **2013**, *2*, 862–870.
- 1003 (38) Cruz-Orive, L. M.; Weibel, E. R. Recent stereological methods for cell biology: A brief
1004 survey. *The American journal of physiology* **1990**, *258*, L148-56.
- 1005 (39) Gundersen, H. J.; Jensen, E. B. The efficiency of systematic sampling in stereology and
1006 its prediction. *Journal of microscopy* **1987**, *147*, 229–263.
- 1007